Adaptive Radiotherapy
CBCT Based Dose Calculation

Master Thesis

Stine Camilla Claessen

Kongens Lyngby, July 2012
IMM-MSc-2012

Technical University of Denmark
Informatics and Mathematical Modelling
Building 321, DK-2800 Kongens Lyngby, Denmark
Phone +45 45253351, Fax +45 45882673
reception@imm.dtu.dk
www.imm.dtu.dk IMM-MSc-2012

Herlev Hospital of Denmark
Oncology Department
DK-2730 Herlev hospital, Denmark
Phone +45 38 68 91 92
www.onkologi@heh.regionh.dk Oncology Department-MSc-2012

Abstract

Background: The aim of this report is to evaluate, if CBCT can be used for dose calculation. The advantage in using CBCT for dose calculation, is to be able to predict and assess the dose delivered to the patient on a daily basis.

Materials & Methods: The study was subdivided into three parts. Part A: Various scan parameters and phantom configurations were investigated for their impact on the Hounsfield units (HUs) for Computed tomography (CT) and CBCT. For this investigation a CIRS water equivalent electron density phantom (DP) was used. The different configurations of the DP were used to obtain HU-relative electron density calibration curves. The CT curve from the CT scan obtained with clinic standard parameters (CTS) was used as reference. Part B: The default and the obtained calibration curves from the different CBCT protocols were selected for the dose calculation on the CBCT images. Using the Alderson phantom it was investigated which protocol and calibration curve was the most appropriate for the CBCT based dose calculation. Part C: The results from the Alderson (ARP) study were evaluated in a clinical perspective on an head and neck patient (H&N) treated with intensity-modulated radiotherapy. In order to investigate if a site-specific calibration curve for different patient groups was needed different calibration curves were used for the head and neck patient. The calibration curves obtained from the pelvis configuration on DP were used to calculate the dose distribution on the pelvis patient treated with rapid arc. The intention was to investigate if CBCT can be used for dose calculation for this patient group.

Results: Part A: Compared to CT it was found, that the HUs from CBCT were more easily affected when changing the scan parameters. Voltage, DP size and insert arrangements affect the HUs the most. Part B: The ARP study showed a maximum dose difference of 0.6% when comparing the use of the

CTS and the default calibration curve. The most appropriate CBCT based dose calculation was achieved with the standard dose head protocol. A 0.3% maximum dose difference between CBCT and CT was found. It was found that further investigation is needed in order to evaluate whether the CBCT or the CT calibration curve achieves the most accurate CBCT based dose calculation. Part C: For the H&N patient a 1.7% maximum dose difference between using the CTS and the default calibration curve was detected. A maximum dose difference between CT and CBCT was found to be 0.3%. As for the ARP study, a further investigation is needed in order to evaluate whether the CBCT or the CT calibration curve achieves the most accurate CBCT based dose calculation. The results for cervix showed that further investigation was needed to conclude whether CBCT can be used for dose calculation on cervix patients. Further it was found that using a site-specific calibration curve for different patient groups achieved a CBCT based dose distribution most similar to the CT based dose distribution.

Conclusion: It is concluded that CBCT can be used for dose calculation on H&N patients, but that further investigation is needed for the cervix patient. The standard protocol for CBCT is shown the to achieve a dose calculation similar to that of CT for the H&N patient. Also, it is concluded that the use of site-specific calibration curve is needed in order to calculate an accurate dose distribution on CBCT.

Summary

Baggrund: Formålet med denne opgave er, at evaluere om cone-beam computed tomography (CBCT) kan bruges til dosis beregning. Fordelen ved at anvende CBCT til dosis beregning er at kunne forudsige og vurdere den dosis der leveres til patienten dagligt.

Materiale & Metode: Dette studie er opdelt i 3 studier. Del A: Forskellige scannings parametre og phantom konfigurationers påvirkning på Hounsfield enhederne (HUs) undersøges for Computed tomography (CT) og CBCT. Til denne undersøgelse anvendes CIRS vand ækvivalent elektondensitetfantomet (DP). De forskellige konfigurationer af DP er anvendt til at konstruere HU-relativ elektrodensitet kalibrerings kurver. CT kurven dannet fra CT skanningen lavet med kliniske standard parametre (CTS) var anvendt som reference. Del B: Default og de kontruerede kalibrerings kurver dannet ud fra de forskellige CBCT protokoller er valgt til at beregne dosis med på CBCT billederne. Ved brug af Alderson fantomet undersøges det, hvilken scanning protokol og kalibreringskurve der er bedst anvendelig til beregning af dosis på CBCT. Del C: Resultaterne fra Alderson studiet blev evalueret i et klinisk perspektiv på en hoved- og halspatient behandlet med intensitet-moduleret stråleterapi. For at undersøge om der var behov for anatomi-specifik kalibreringskurve for forskellige patientgrupper blev forskellige kalibreringskurver anvendt på hoved- og halspatienten. Kalibreringskurverne dannet fra pelvis konfigurationen af DP blev anvendt til at beregne dosis på pelvis patienter behandlet med rapid arc. Formålet var at undersøge om CBCT kunne bruges til dosis beregning på denne patientgruppe.

Results: Del A: I forhold til CT, blev det fundet at HU fra CBCT var lettere påvirkelige når skanningsparametrene blev ændret. Spænding, DP størrelse and *insert arrangements* påvirkede HU mest. Del B: ARP studiet viste en maksimum dosis forskel på 0.6% ved brug af CTS og default kalibrerings kurve. Den mest

hensigtsmæssige dosis beregning på CBCT opnås ved brug af *standard dose head protokol*. En 0.3% maksimum dosis forskel blev fundet mellem CBCT og CT. Det kunne konkluderes, at der kræves en nærmere undersøgelse for at kunne evaluere om en CBCT eller en CT kalibreringskurve opnår den bedste dosis beregning på CBCT. Del C: For H&N patienten blev der fundet en 1.7% maksimum dosis forskel når CTS og default kalibreringskurven bruges var fundet. En maksimum dosis forskel mellem CT and CBCT blev fundet til 0.3%. Som ved ARP studiet blev det konkluderet at en nærmere undersøgelse kræves for at undersøge om CBCT eller om CT kalibreringskurven opnår den bedste CBCT dosis beregning. Resultaterne for livmoderhalskræftpatienter viste at en nærmere undersøgelse er påkrævet for at kunne konkludere om CBCT kan bruges til dosis beregning for livmoderhalskræftpatienter. Det blev endvidere undersøgt om, anatomi-specifik kalibreringskurve for forskellige patientgrupper opnår en CBCT baseret dosis beregning tæt på dosis beregning af CT.

Conclusion: Det blev konkluderet at CBCT kan bruges til dosis beregning af H&N patienter, men at en nærmere undersøgelse er påkrævet for livmoderhalskræftpatienterne. Standard protokollen for CBCT viste sig at være den bedst egnede til at opnå en CBCT dosis beregning tæt på CTs for H&N patienten. Det er også konkluderet at brugen af en anatomi-specifik kalibreringskurve er nødvendig for at kunne beregne en nøjagtig dosis beregning på CBCT.

Preface

This M.Sc. thesis is written by Stine Camilla Claessen. It was prepared in the spring 2012 at Copenhagen University Hospital, Herlev, the Department of Oncology (R). The work has been carried out in co-operation with the Department of Informatics and Mathematical Modelling at the Technical University of Denmark. This project account for 30 ECTS points and is in fullfilment of the requirements for acquiring a M.Sc. in Medicine & Technology at the Technical University of Denmark (DTU) and the University of Copenhagen (KU).

Herlev, 27-July 2012

Master Thesis
Stine Camilla Claessen

Acknowledgements

I want to thank my supervisors, Claus Behrens, David Sjöström, Eva Emma Maria Sjölin and Rasmus Poulsen for their guideance. They have all been very patient, supportive and their encouragement helped me through the research and writing of this thesis. Moreover, I wish to thank the staf, at the Department of Oncology (R), Herlev Hospital for their kind help. I also wish to thank Sune Kristian Buhl (Herlev Hospital) for his help with the use of the treatment machine. A special thank goes to Eva Emma Maria Sjölin (Herlev Hospital) for her enthusiasm, inspiration and help provided on using TPS throughout this project.

Furthermore, I wish to thank my co-students, Marie Elgaard Korsholm Nielsen and Rikke Eiland for their support and constructive feedback on my ideas and thoughts. A special thank, goes to Hans Martin Kjer (co-student) for his great help in programming, latex, constructive feedback and great company. I would also like to express by gratefulness to all those who looked closely at the final version of the thesis for grammer and improvement.

Finally, a special thanks goes to my family and friends for their support throughout this project. Especially, I would like to thank my boyfriend Thomas Lyster Legald and my mother Lisbeth Lene Claessen whose patient love enabled me to complete this work.

Contents

List of Figures

List of Tables

List of Abbreviations

Abbreviation	Description
AAA	Anisotropic Analytical Algorithm
ART	Adaptive Radiotherapy
CBCT	Cone Beam Computed Tomography
CT	Computed Tomography
CTV	Clinical Target Volume
DAHANCA	Danish Head and Neck Cancer group
DICOM	Digital Imaging and Communication in Medicine
DP	Density Phantom Referres to the CIRS Phantom
DRR	Digitally Reconstruction Radiographs
DVH	Dose Volume Histogram
FOV	Field of View
FPD	Flat Panel Detector
HDP	Head Density Phantom, the Inner Part of the CIRS Phantom
PDP	Pelvis Density Phantom, the entire CIRS Phantom
RED	Relative Electron Density
GTV	Gross Target Volume
Gy	Gray (J/kg)
H&N	Head and Neck
HU	Hounsfield Unit
ic	Referring to the Inserts in the Inner Circle of the CIRS Phantom
IMRT	Intensity Modulated Radiation Therapy
IGRT	Image Guided Radiation Therapy
keV	Kilo Electron Voltage

kV	Kilo voltage
LINAC	Linear Accelerator
mA	Milli Ampere
MU	Monitor Units
OAR	Organs At Risk
OBI	On-Board Imaging
oc	Referring to the Inserts in the outer circle of the CIRS Phantom
PET	Positron Emission Tomography
PRV	Planning Organ at Risk Volume
PTV	Planning Target Volume
RA	Rapid Arc
SNR	Signal-To-Noise-Ratio
STD	Standard Deviation
TPS	Treatment Planning System
VOI	Volume of Interest

Chapter 1

Introduction

Cancer in the head and neck region (H&N) as well as in the pelvis region can be treated with radiation therapy (RT). However, this therapy it not without risks. These regions contain some critical organs, which are important for maintenance of the human well-being. Radiation destroys healthy tissue, and sometimes to an extent, so that it damages the functions of the organs and thereby interrupt the well-being of the patient. To avoid these damages as much as possible, an individual treatment plan is made. This plan is made on basis of a computed tomography (CT) scan in a way that reduces the radiation to the healthy tissue and takes the critical organs into consideration. RT can results in anatomically changes of the patient and in some situations result in a treatment plan that no longer fits the patients anatomy. If no correction is carried out, the healthy tissue and the critical organs can receive too much radiation, and the tumour can receive lesser radiation than planned [19, 29, 37].

A method of evaluating if the treatment has caused anatomical changes, and to what extent they have occurred, is to make a Cone-Beam Computed tomography (CBCT) scan. CBCT is acquired by the treatment machine and contains the patient´s actual anatomy. Comparing CBCT with CT, anatomical changes can be detected and a decision can be made whether a new treatment plan is required or not. This report will investigate, if the dose can be calculated on CBCT and thereby increase the efficiency of the imaging process of the treatment planning. This will benefit the patient and reduce the ressources used for optimizing the treatment plan. The use of CBCT, will also provide the option of evaluating

the dose delivered to the patient on daily basis [45]. There are, however, some issues of concern when using CBCT scans, such as the poorer quality due to scatter and variation in the Hounsfields units (HU)[34].

The aim of this study is to investigate, if it is possible to obtain a CBCT based dose distribution which is as accurate as the CT based dose distribution. Furthermore, using CBCT for dose calculation, if it is accurate enough, makes it possible to predict and assess the dose delivered to the patient on a daily basis and use it for adaptive RT [45].

Chapter 2

Theory

2.1 The Course of RT

Cancer can be treated with surgery and/or radiotherapy with or without chemotherapy, or just chemotherapy [22]. This chapter will describe the RT planning process (Figure 2.1).

Figure 2.1: The treatment planning process for RT.

2.2 Patient Immobilization

The patient receives the radiation in fractions. Delivering the prescribed dose in small doses over a period of time allows the healthy tissue to recover, but it also increases the risk of set-up errors between the fractions [9, 32]. It is therefore important before initializing the RT to determine the position of the patient and be able to reproduce the set-up of the patient from one treatment to another.

The patient is immobilized on the treatment couch with different devices depending on where the tumour is localized. Some of the simplest immobilization devices used in RT are velcro belts, elastic bands and headrests. The latter serves for patient comfort during treatment. A thermoplastic mask is used for H&N cancer patients (Figure 2.2 Left). It is custom made and attached to the treatment couch [20, 30, 22]. For pelvis cancer patients vacuum based immobilization devices are often used due to its reusability (Figure 2.2 Right). A pillow filled with small beads is placed around the treatment area. A Vacuum pump then evacuates the pillow which leaves the patients form as an imprint on the pillow [30].

Fixation of the H&N Fixation of pelvis

Figure 2.2: Immobilization devices. Left) A custom made thermoplastic mask used for immobilization of H&N cancer patients [1]. Right) A vacumbased form for the pelvis cancer patients, [2]

.

2.3 Image Acquisition

A computed tomography (CT) scan is taken of the patient in the treatment position with the immobilization device. This CT scan is used for the later treatment planning. The treatment couch and a laser system available in the room are used to help precisely positioning the patient. CT is the most common image modality for making treatment plan. However it is often used together with other scannings modalities. Magnetic resonance imaging (MRI) creates a ful 3D image of the tumour such as with CT, but provides a better soft-tissue contrast. CT and MRI can be complementet with positron emission tomography (PET) [32, 22]. The use of different image modalities provide a more complete information about the patient [46].

2.4 Volume Delineation

The step before designing the treatment plan is to delineate the target volume and organs at risks (OARs). The intention is to ensure, that the taget volume receives the prescribed dose and to protect the OARs against irradiation. Especially in the H&N region there are many OARs such as medualla, brain stem, salivary gland and optic nerve [32, 22]. At Herlev Hospital the delineation of structures is carried out in a treatment planning system (TPS) (Eclipse, Varian Medical System v. 10.0 [40]) and performed by a radiation oncologist and a radiologist. The target volumes and OARs, are delineated on the acquired CT scan. If structures are hard to visualize on the CT, the structures can be drawed on a MRI or on a PET [11, 32]. The structures on the MRI or PET can then be transferred to the CT after registration of the images. Organs with well-defined boundaries are delineated automatically or semi-automatically. If the organs do not have well-defined boundaries, a fully manual delineation is required. The contours are manually drawed slice by slice.

2.4.1 Definition of Volumes

This section describes the delineated volumes related to the tumour and OAR, which are used for the treatment planning (Figure 2.3).

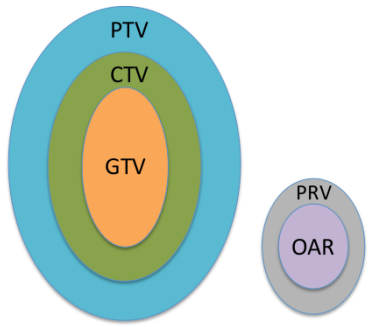

Figure 2.3: Delineated Volumes

Gross Tumour Volume: Gross tumour volume (GTV) is the volume consisting of visible or palpable tumour mass and metastasses. This volume is often defined on basis of clinical examination and on imaging techniques such as CT, MRI and PET [5].

Clinical Target Volume: In som cases lymphnodes or other tissue can be effected or considered to be at risk and require treatment. In these cases it is nessesary to include a margin around GTV. A CTV can also exist without including a GTV [5, 18, 30]. CTV is often determined by an radiation oncologist based on biological knowledge and on knowledge of the clinical behaviour of the specific tumour [30].

Planning Target Volume: The planning target volume (PTV) is intended to ensure that CTV receives the prescribed dose [5]. The PTV is often used to cover one or several CTVs and include a safety margin (CT + safety margin) [30]. The margin is intended to account for uncertainties in the patient set-up, anatomically changes related to size, movement and shape of the tumour as well as penumbra [5, 18].

OARs: OARs refer to normal tissue within the region or close to the region receiving radiation. OARs are sensitive to irradiation and is in risk of being damaged by radiation. Special care must therefore be taken into account when designing the treatment plan. Guidelines concerning the dose contrains for the OARs are followed when designing the treatment plan. These guidelines consist of tolerance levels for the delivered dose [5, 30]. To further ensure that the delivered dose to the OARs do not exceed these tolerance levels, a margin is set around the volume of the OARs. This margin is referred to as the planning risk volume (PRV). The intention with this margin is, as for PTV, to account for uncertainties in the patient set-up and the motions of the internal organs [5, 18].

2.5 Treatment Planning

The design of the treatment plan is carried out in the TPS, which can simulate the treatment delivery (treatment technique and dose distribution) of the linear accelerator (LINAC) (Section 2.6) [30].

Construction of the treatment plan includes descisions about the beam geometry and the beam arrangement. The beam arrangement is designed by dosimetrists or medical physicists. It consist of a number of fields from different angels and with different intensities (Figure 2.4). The composition of these fields depends on the selected delivery technique and on the pre-delineated structures (Section 2.4). The beam arrangement is constructed so as to ensure that the tumour receives sufficient radiation while protecting the OARs [30]. After the beam

geometry and beam arrangement have been designed, a rough optimization is performed.

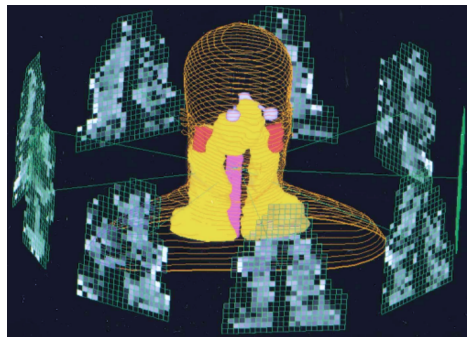

Figure 2.4: A 3D representation of a patient with the structureset treated with IMRT. The structure set contains: PTV (Yellow area), spinal cord (Pink area) and parotid gland (Red area). The non-uniform intensity profiles of the beams are used to generate the dose distribution. Adapted from [43]

The dose distribution is calculated in TPS with the intention to assess and predict the delivered dose. The treatment plan is optimized based on the dose contrains. This is done to achieve tumour coverage and minimize the dose delivered to the OARs. An evaluation of the treatment plan can be carried out by dose volumen histograms (DVHs) (Section 2.10), the isodoselines [1] or the dose distribution showned in a color wash, where hot spots [2] can be detected. The last step of the treatment planning process is to approve the plan [30, 32].

2.6 Treatment Delivery

The RT is conducted using a LINAC (Figure 2.5). The gantry of the LINAC can rotate 360° around the patient. This advanced technology makes it possible to deliver radiation to the tumour from any angle. Furthermore the LINAC is capable of acquiring kV images of the patient before treatment, as CBCT (Subsection 2.7.2). Before the RT, the patient is set-up with the immobilization device and positioned with the moveable couch and a laser system available in the treatment room. Furthermore a 2D or a 3D match is used to verify the

[1] Isodoseline: Connection between points receiving the same dose. Provide a planer representation of the dose distribution.

[2] Hot spots: Areas receiving an unacceptable high dose

patient set-up [32]. The intention with the set-up is to minimize set-up errors to achieve a more accurate dose delivered to the patient [32].

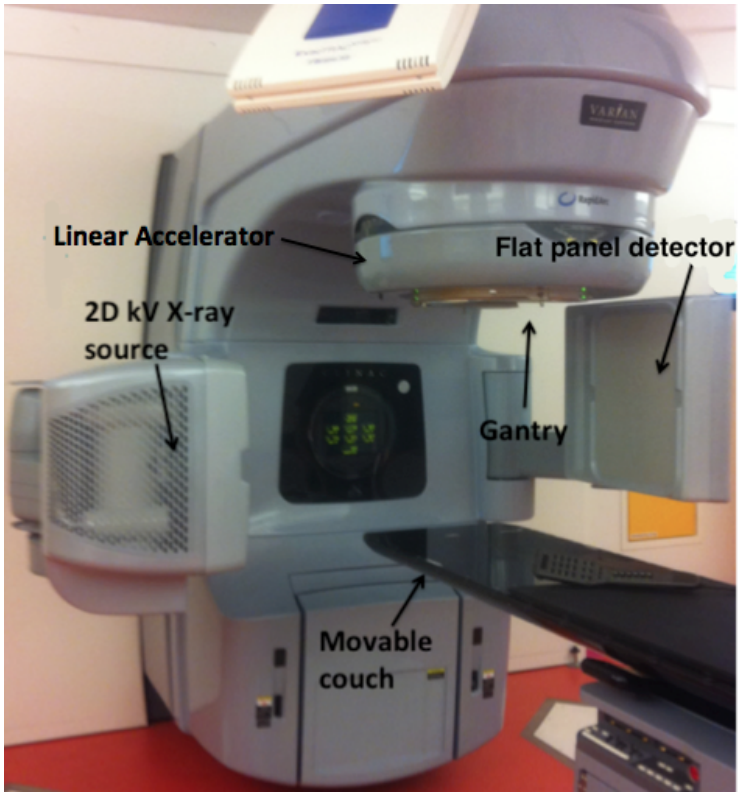

Figure 2.5: The Varian Clinac iX treatment unit.

The LINAC can for example deliver both intensity modulated RT (IMRT) and rapid arc (RA). IMRT is a technique, which has the ability to achieve a high degree of target conformity and to protect healthy tissue. This is acccomplished using non-uniform radiation beam intensities delivered to the patient (Figure 2.4) [43].

The radiation is given from several static angles (Figure 2.6 a). This technique often uses (5-9) beams positioned around the patient at different angles. The beam is modulated by dynamic multileaf collimators (MLC) (Figure 2.6 b). The leaves of the MLC can move independently and slides in and out to shape the beam. The beams are modulated so that the largest amount of radiations is delivered to the target in areas, where the OARs are least affeceted. Due to IMRTs ability to protect OARs close to the tumour it is commonly used for

H&N cancer patients [43].

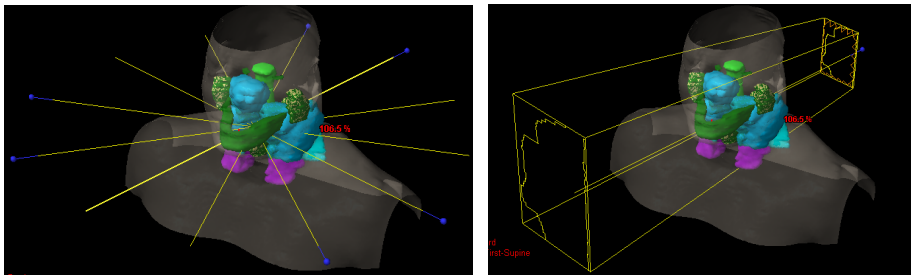

Figure 2.6: Left) 3D presentation of a H&N patients with structures and six fields used for IMRT. The fields are presented as lines. Right) 3D presentation of one of the fields presented as a cone and the MLCs.

RA is a volumetric arc therapy and is an improvement of IMRT. The radiation is delivered with a continuously varying beam as the gantry rotates around the patient (Figure 2.7). The advantages of the RA technique, is that it is faster to deliver [41].

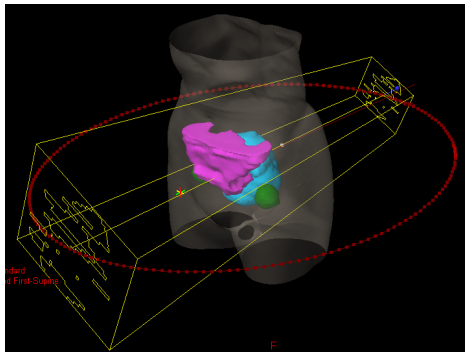

Figure 2.7: A 3D simulation of a cervix patient with a structure set treated with RA. The structure set contains: PTV (Blue area), caput femoris (Green area) and Intestine (Pink area). The red circle indicates the gantry motion around the patient. The yellow lines present the beam at a specific position and the MLCs.

2.7 Image Modalities

This chapter describes the principles behind computed tomograpy (CT) and conebeam CT (CBCT). The two image modalities will be compared and their advantages and disadvantages will be described.

2.7.1 CT

CT is an image modality showing a cross-sectional view of the patient. It has through the years proven to be an irreplaceable diagnostic tool not only in RT but in many different medical applications. Most of the scanners of today utilize a fan-shaped X-ray source in a helical progression to make the image slices [35, p. 2]. Although the helical CT scanner is a more advanced scanner, the images are still based on the same basic CT principles: The CT image is constructed by rotating the X-ray tube 360° around the patient while emitting X-rays. Opposite the X-ray tube one (or more) multiple ring detector arrays are located and receives the intensity of the attenuated X-rays (Figure 2.8 Left). The intention of using multiple ring detector arrays are to acquire a full body scan and a high image resolution. This type of detector also shorten the scan time [8, p. 327-331], [25, p. 18-31]. The data is then reconstructed into a 3D image. For this purpose different algorithms exist, but the best known is the filtered back projection algorithm[8, p.353],[12, p.79].

The reconstructed image matrix is composed of voxels. To each voxel, a value representing the attenuated X-rays passing through it, is attached. A slice of the reconstructed image is therefore composed of pixels representing the voxels in the patients anatomy (Figure 2.8 Right). Each of these voxels is displayed as a HU relative to water. In other words, HU indicates how much the x-rays passing through that voxel are attenuated through the tissue [8, p. 356], [25, 31-32]. In the X-ray energy spectrum for constructing medical images <100 kV two primary interactions occure Comptom scatter and photoelectric effect [8, p. 38-45].

With an average X-ray energy of 75 kV, Comptom scatter dominates the X-ray attenuation. Compton scatter is influenced by the physical properties of tissue, such as the electron density and the atomic number (Figure 2.9) . The image contrast is dependent on these physical properties. The image contrast is obtained by the differences in attenuation of X-rays (Figure 2.9). The detectors

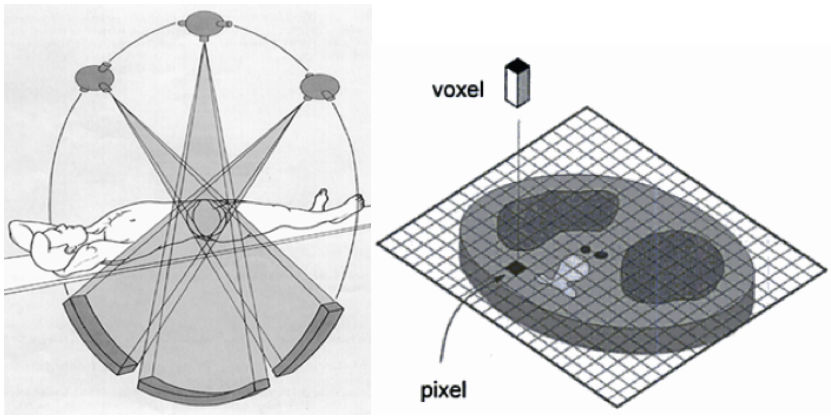

Figure 2.8: Left) CT scan of a patient using multiarray detector seen from different angels, adapted from [25]. Right) CT makes transverse cross-section images. Every pixel in a slice of the cross-sectional image represent a voxel in the image, adapted from [25, page. 19]

receive both primary X-rays and scattered X-rays. Scattered X-rays results in incorrect HUs and carry only little or no information about the patient. It is therefore important to eliminate scatter as much as possible [8, 356-357, 363] [25, p.31-34].

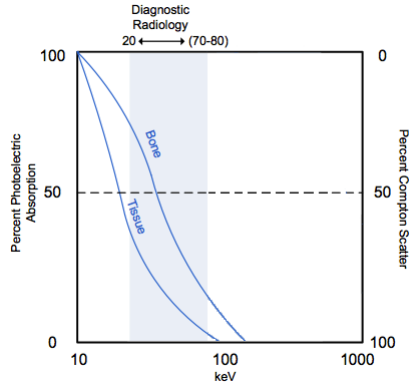

Figure 2.9: The percentual contribution of photoelectric effect and Compton scatter for different X-ray energies. Photoelectric effect predominate for low x-rays energies and for materials with high atomic number such as bone. Compton scatter predominate for high X-rays energies and for materials with low atomic number such as tissue. Modified from[8]

2.7.2 CBCT

This technology may be used for diagnosis, clinical application and treatment evaluation. CBCT uses a cone-shaped X-ray beam which incorporates the entire field of view (FOV) by a single rotation of the source and detector. A conventional CT scanner apply a fan-shaped X-ray beam where several slices are obtained to incorporates the FOV [26, 35] (Figure 2.10).

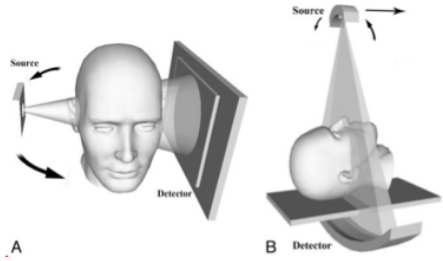

Figure 2.10: Different scans modes: Left) CBCT uses a cone-shaped X-ray beam. Right) CT uses a fan-shaped X-ray beam, adapted from [28]

Compared to the the multi ring detector arrays in conventional CT, CBCT

images are detected by a high spatial resolution 2D flat panel detector (FPD) [23, 26, 35]. Another difference to conventional CT is that CBCT has no collimator in front of the detector array. CBCT also has a limited scan range in the superior-inferior direction.

Due to the cone-shaped beam and no beam collimator, the 2D FPD will detect more scatter from the entire object than conventional CT (Figure 2.11). The high spatial resolution detectors are also more sensitive to small movements and thereby motion artefacts compared to CT. The noise, artefacts and scatter reduce the image contrast and the signal-to noise ratio (SNR) (Figure 2.11). This complicates the usability of CBCT for dose calculation [14, 26, 28, 35, 36].

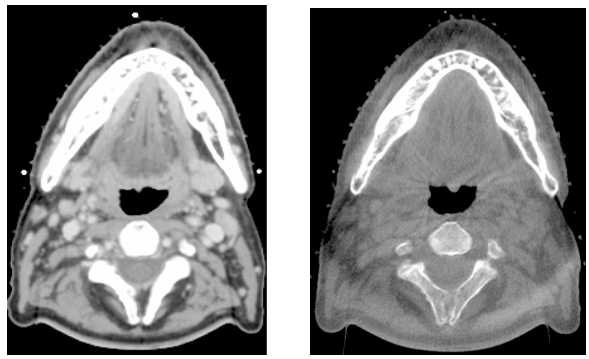

Figure 2.11: H&N: Left) Conventional CT scan. Right) CBCT scan

The major advantage of using CBCT in RT is that it can be mounted on the gantry of the radiotherapy machine. CBCT is generated before or after the actual treatment and can be used for patient set-up and adaptive RT (Section 2.11).

2.8 Bowtie Filter

Two acquisition modes are available in the OBI system for CBCT: Full fan mode and half fan mode (Figure 2.12) [39]. The full fan mode with its smaller FOV is used for smaller objects, such as the head region. The half fan mode only views parts of the object at one projection. This mode is therefore recommended for larger objects, such as the pelvis region[42].

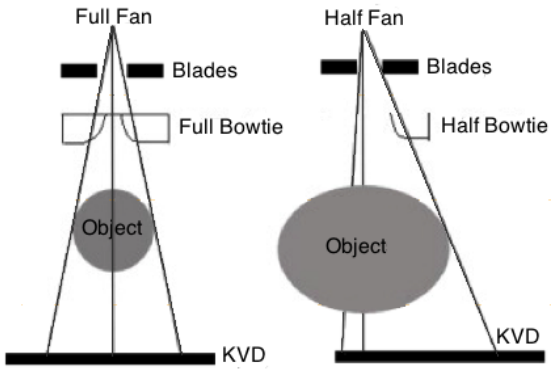

Figure 2.12: CBCT aquisition modes. Left) Full fan mode with full bowtie filter mounted. In this mode the kilovoltage detecetor (KVD) (flatpanel) is centered. Right) Half fan mode with half bowtie filter mounted. In this mode the KVD is shifted to one side and covers more than half the patients volume, Modified from [42].

The x-ray beam is attenuated less, at the boundary of the patient than in the middle because it travels through less tissue. In order to reduce skin dose and improve the image quality by reducing x-ray scatter, a bowtie filter can be used (Figure 2.13). To achieve a more homogen image a so called bowtie filter is used. This filter is shaped In this way so, that it decreases the beam intensity, where the x-rays travels through less tissue [42].

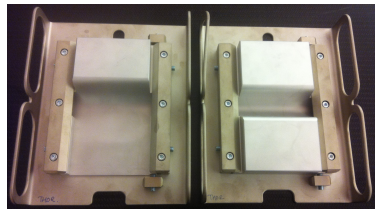

Figure 2.13: Bowtie filters available with the OBI system: Left) Half bowtie filter. Right) Full bowtie filter

The bowtie filter is made of aluminum and is mounted in front of the kV x-ray source. Two bowtie filters can be used with the OBI system : A full bowtie filter and a half bowtie filter [39]. The full bowtie filter is used with the full fan mode because this mode enclose the entire object. The half fan mode covers only a part of the object at one projection. This half bowtie filter is therefore used with the half fan mode.

2.9 Calibration

The HU is not unique for a given material, but is dependent on among other thing the scanner and on the scanning protocols. The HUs therefore can not directly be used for dose calculation[14]. The algorithms used for dose calculation in TPS converts the HUs into relative electron densities based on a HU-to-RED map. In order to use CT and CBCT for dose calculation it is nessesary to relate the HUs for the specific scannert o the actual RED. [21, 23, 33, 38, 45]. The relationship between the HUs and REDs is well represented by a two-piece linear fit (Figure 2.14) [21]. This HU-to-RED map will in the following be presented as a calibration curve.

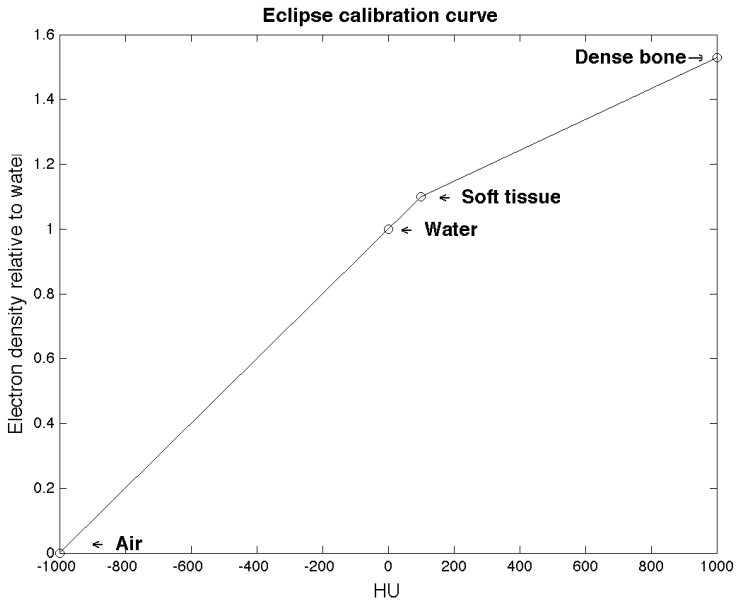

Figure 2.14: The default calibration curve available in TPS (Eclipse, Varian Medical System v. 10.0)

2.10 Dose Volume Histogram

A 3D treatment plan contains a large amount of dose information. This complicates the evaluation. One way to easily summarize the 3D dose distribution

information is to condense it into a 2D DVH. DVH is an evaluation tool which is often used for treatment plan evaluation[30].

There are two types of DVHs, differential and cumulative. For clinical purposes the cumulative is more useful [15]. A differential DVH is very similar to a typical histogram. It shows the relative or absolute volumen in the dose interval. A Cumulative DVH on the other hand presents the percent of volume receiving a dose equal to or greater than that dose (Figure 2.15). In the following DVH will be refer to as the cumulative DVH.

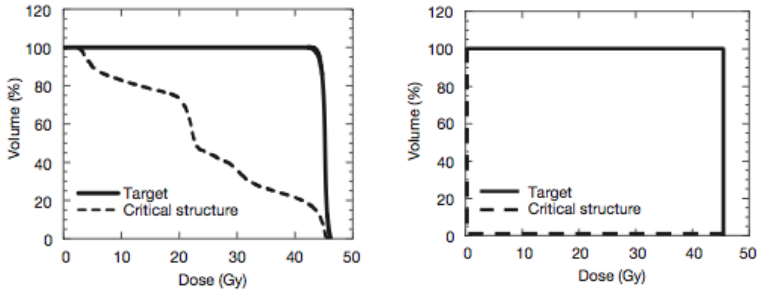

Figure 2.15: Cumulative DVH. The first bin which is 0 Gy will always contain 100 % of the volume because the volumen receive at least 0 Gy. The last bin in the graph will contain a volume receiving that dose or more. Left) Illustrates an exampel of realistic DVHs for target and critical structures. Target receives maximum dose to almost 100% of its volumen. Right) Ideal DVHs for target and critical structure. For the target 100 % of the volume receives the prescribed dose. For the critical structures 100% of the volume receives zero dose [30].

DVHs is used to assess the treatment plan. Based on DVHs it can be evaluated, if the target volume receives a uniform dose throughout its volume. This uniformity is displayed as a steep slope. Furthermore it can be evaluated, if the OARs receive a dose that exceeds the dose constrains. The dose distribution from the CT and CBCT can be compared and evaluated using dose statistics [15].

The typically evaluated DVH points for PTV in accordance with the recommendations from the ICRU Report 83 [44] are:

- $D_{2\%}$, The near maximum dose, which is the dose received by 2% of the volume.

- $D_{98\%}$, The near minimum dose, which is the dose recieved by 98% of the volume.

The dose estimates, D_2 and D_{98} are more accurate estimates compared to D_{max} and D_{min}. These dose estimates are affected less by outliers in the dose values and can be seen as alternative to the maximum and minimum dose estimates. D_{98} can be used to determine if low-dose areas are present in the target volume. D_2 is a more clinical alternative to D_{max} in order to detect the maximum observed dose by the target volume or OARs. Another dose estimate which can be used to evaluate the dose distribution is, D_{mean} the average absorbed dose in the target volume. This dose estimate cannot be determine from the DVH [15].

Based on the DVH it can also be evaluated, if the OARs receive a dose within the recommended constrains which are organ specific. The tissue of medulla is serially arranged. If some of its tissue gets damage it will become dysfunctional. In the worst-case scenario if medulla is damaged due to RT, the patient can be paralyzed [17] or develop myelopathy [3] [16]. When evaluating medulla, using the maximum absorbed dose value (D_{max}) is therefore recommended [44]. For parotis, D_{mean} is often used as the dose constrains [15]. The reason for this is, that the tissue of parotis is parallelly arranged and its function can remain even though, some of its tissue is damaged [44].

Volume estimates are also points from the DVH. For exampel V_{45Gy} indicates the volume (V) receiving 45Gy or more [15].

[3] Myelopathy: Disease of the spinal cord

A disadvantage of DVHs is that they do not provide spatial information of the dose in relation to structures. They only provide information about the dose distribution within a structure. Location of under-dosed and over-dosed areas in the structure can therefore not be detected by DVHs. Despite of that, DVHs is a quite easy tool for evaluating the treatment plans [13, 15].

DVH points to be evaluated depend on the volume of interest and thereby on the dianostic group. The DVH points used for the comparison of the dose distribution will therefore be introduced in the section related to two diagnostic groups in this thesis (Section 6.2 and 7.1.3).

2.11 Adaptive RT

The goal of RT is to obtain tumour control [4] while sparing healthy tissue in order to minimize side effects. The size, shape and location of organs can change during treatment, due to normal organs anatomy variability and RT. When exposing the patient to radiation weight loss and tumour shrinkage can be observed. These anatomically modifications can lead to differences between the planned and delivered dose to tumour and surrounding healthy tissues. This can effect tumour control and OARss in a way, that tumour receives a reduced dose and the OAR an increased dose [7, 9, 19].

Image guided RT (IGRT) is the use of images for patient set-up. These images are obtained in the treatment room prior to irradiation. The intention of the images are to acquire anatomical information of the patient in order to improve the quality of the treatment. CBCT imaging provides a 3D image of the patient, which can be used for patient set-up and detection of anatomically changes [10, 24]. A study by O´ Daniel et al. [29] found that without IGRT the dose to parotis gland increases significant in 45% of the patients. In contrast to using IGRT where the dose is reduced in 91% of the patients.

The patient is immobilized on the treatment couch before each treatment fraction. Patient motion can though still be detected from fraction to fraction. By adjusting the patient position it is not possible to correct for all anatomically changes [9]. A way to correct for anatomically changes is to adjust the treatment plan based on a new CT image. Images obtained during treatment can be used to make such an adaptive treatment plan. This process is adaptive RT

[4] tumour control: The tumour receives radiation which kills the tumour cells.

[10]. From a study by Hansen et al.[19] it is found that without re-planning the target receives a reduced dose and the healthy tissue an increased dose.

The need for Adaptive RT (ART) has grown with the development of more advanced techniques such as IMRT and RA. These Techniques have the ability to deliver highly conformal dose and with its steep gradient between the targets and OARs, they are sensitive to anatomically changes. This may increase the risk of inaccurate dose distribution. ART is also necessary if the margins between PTV and OARs are small. In these cases ART has the ability of minimizing the risk of overexposing healthy tissue and OAR and/or underexpose target [9, 24].

Chapter 3

Previous work

Several articles about CBCT based dose calculation exist. Three related studies will be described in the following. These three articles, serves as inspiration for the method and materials for constructing calibration curves and the use of these curves for dose calculation.

Y. Rong et al. [34] describes the use of CBCT for dose calculation compared to CT. The study uses the CIRS model 062 phantom as used in this thesis (Figure 5.1). The CIRS phantom is sandwiched between two 5 cm thich squared water blocks with the intention of simulating the actual patient situation (additional scatter). Y. Rong et al. investigates the effect of varying current: 20, 40 and 80 mA. The phantom size and its inserts arrangements effect on the HUs and dose calculation are also investigated. Furthermore the effect of using different calibration curves for the same phantom is examined. The RANDO head phantom is used to evaluate the constructed calibration curves and for the CBCT dose calculation (Figure 6.2). The calculated dose distributions are then then evaluated by comparing DVHs PTV and OARs.

Y. Rong et al. finds, that using a calibration curve for a corresponding body part achives a 2% maximum dose difference between CBCT and CT. Additionally it is observed that using the HDP calibration curves for other body parts, a dose error of 3% or higher between CBCT and CT can occur. CBCT based dose calculation is found feasible when using site-specific calibration curves [34]. Compared to the study peformed by Y. Rong et al. the CIRS phantom is

scanned in water in this study. Beside from the current, the effect of varying voltage and millisecond on the HUs are also investigated. Furthermore this study investigates the use of different scan protocols for the CBCT based dose calculation. In contrast to the study peformed by Y. Rong et al. patients are also used for the evaluation in this study.

Y. Yang et al. [45] evaluates the achievable accuracy in CBCT based dose calculation. A modification of the CBCT (mCBCT) is carried out. The modification is performed by mapping the HUs from CBCT with the HUs from CT. A phantom, three prostata patients and one lung patient are used for evaluation of the dose distributions.

Y. Yang et al. observed dose differences less than 2% between CBCT and mCBCT in the three prostata cases. Based on these results Y. Yang et al. concluded that CBCT can be used directly for dose calculation. For the phantom a dose difference between the CT and CBCT is found to be within 1%. For all three prostata patients dose differences between CT and CBCT were found to within 3%. For the lung case a 5% maximum dose difference between CBCT and CT is observed. The conclusion of this study is that CBCT can be used directly for dose calculation for prostata patients but not on ung patients [45].

J. Hatton et al. [21] investigate the use of different phantoms for CBCT based dose calculation. The intention is to find the phantoms most appropriate for that purpose. J. Hatton et al. investigate the effect of scanning CIRS with a water equivalent gel bolus (DP with scatter) compared to scanning it in air (DP air).

J. Hatton et al. finds that CIRS model 062 with scatter can be used and is one of the most appropriate phantom for investigation of CBCT based dose calculation. From this study a maximum dose difference of 2-3% between CT and CBCT is found, when using calibration curves obtained from the DP with scatter. This is in contrast to the observed 15% dose difference when calculating the dose distribution from CBCT using the calibration curve when scanning the DP in air. Furthermore it is found that calibration curves obtained from the DP with scatter should be used for dose calculation on phantoms with similar size [21]. Based on the results from this study by J.Hatton et al. [21] most of the CBCT scans of the CIRS phantom is scanned in a container filled with water (additional scatter).

The results of the above described studies [21], [34] and [45] will be discussed with relation to this study in Section 5.3, 6.4, 7.2.2, 7.3.2 and 7.4.2.

Chapter 4

Illustration of this Study

The purpose of this chapter is to introduce the overall method of this study.

This study consist of three parts:

A) Investigating how the different scan parameters influence the HUs which leads to different calibration curves. A selection of the constructed calibration curves are then used in the next two studies (B and C).

B) A phantom study is performed to investigate the use of different CBCT scan protocols for dose calculation. The intension is to investigate which scan settings and calibration curve that results in a CBCT based dose distribution most similar to the CT based dose distribution.

C) A patient study is carried out with the purpose of evaluating the results from the second study (B) in a clinical persepctive. These results are evaluated on two patient categories: one H&N patient and one cervix patient. The H&N patient is also used to investigate the effect of using the calibration curves obtained from two different scan protocols on the dose distribution.

The material and method, results, discussion and conclusion for each of the three studies will be presented sequential.

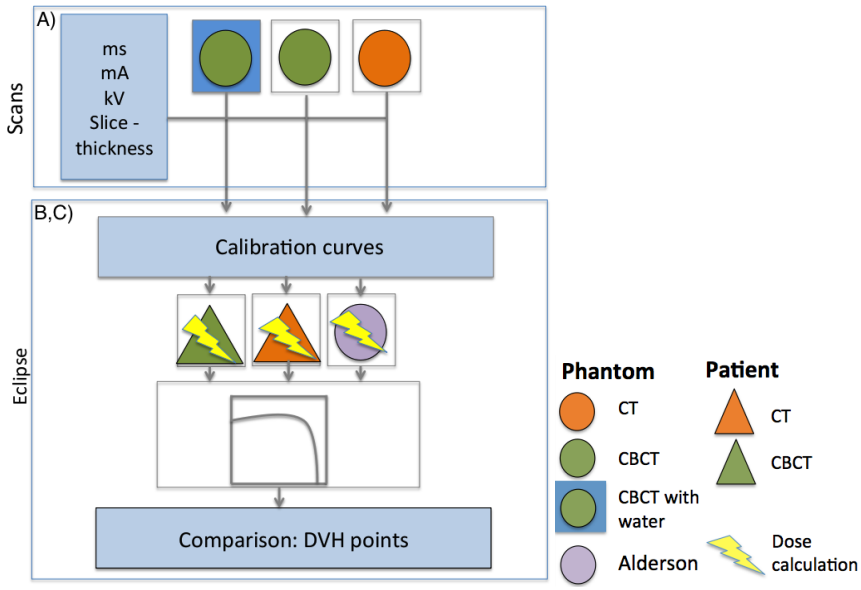

Figure 4.1: A) CBCT and CT scans are performed on a phantom with use of different scan protocols and when varying the scan parameters: ms, mA, kV and slice. Calibration curves are constructed on basis of the obtained CBCT and CT scans. B, C) These curves are used for the CBCT and CT based dose calculation in TPS (Eclipse). The dose calculations are performed on an anthropomorphic phanton (Alderson) and on a H&N and a pelvic patient. DVH points are used for dose evaluation

.

Chapter 5

Part A: Investigation of Scan Parameters

This chapter investigates the influence of scanning with different scan protocols and the impact on the HUs, when varying the scan parameters (Figure 4.1 A).

5.1 Part A: Materials and Methods

5.1.1 Data Specification

To investigate the HU - RED relationship, a phantom with known relative electron densities is used. The CIRS phantom model 062 (CIRS Tissue Simulation Technology, Norfolk, VA, USA) is used for that purpose (Figure 5.1). In the following the phantom will be referred to the density phantom (DP).

The DP is elliptical with a flat base and is 27 cm heigh, 33 cm wide and 5 cm

Figure 5.1: CIRS phantom model 062 [3]

Table 5.1: RED values of the inserts in the DP [3]. High, Soft and Low refer to high, soft and low RED materials.

Materials	RED
Dense bone	1.512 - High
Trabecular Bone	1.117 - High
Liver	1.052 - Soft
Muscle	1.043 - Soft
H20	1.000 - Soft
Breast	0.976 - Soft
Adipose tissue	0.952 - Soft
Lung(Exhale)	0.489 - Low
Lung (Inhale)	0.190 - Low

long. It has 8 different tissue equivalent inserts located at 17 different locations. Each of the inserts has a RED ranging from 0.19 for inhale lung to 1.512 for dense bone (Table 5.1).

The DP has a circular inner section with a diameter of 18 cm and can hold eight material inserts (Figure 5.1) (Table 5.1). The inner part simulates the head and the entire DP simulates the pelvis due to the corresponding sizes. They wil be refer to as the head DP (HDP) and the pelvis DP (PDP). In the following the RED in the inner section of PDP will be referred to as PDP (ic) and the RED in the outer section of PDP as PDP (oc). Using this DP the RED of the tissues are know in advance and a correlation can be found between the RED and HUs[3].

5.1.2 CT Acquisition

CT images of the DP are obtained with a Phillips Brilliance CT Big Bore scanner (Phillips, Amsterdam, the Nederlands) (Figure 5.2). Before the CT scan, the DP is aligned using in-room lasers passing through the center of the DP.

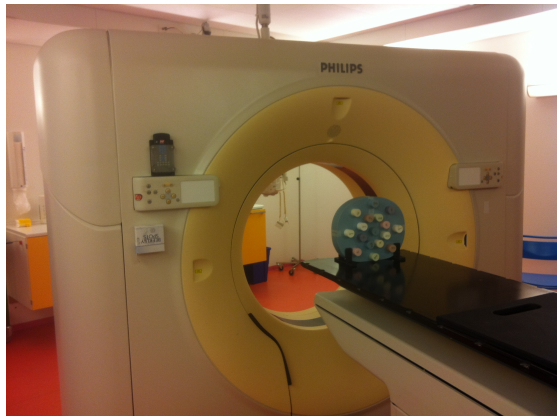

Figure 5.2: Phillips Brilliance CT Big Bore scanner

In order to investigate the size of the DP and the effect of its inserts on the HUs, the CT scans are obtained for both the HDP and PDP. The investigated scan parameters are: kV, mAs and slice thickness (Table 5.2).

Table 5.2: The investigated CT scan parameters. Standard scan settings refer to the parameters used in clinic and are highlighted.

	Head configuration	Pelvis configuration
Scan protocol	Head/neck	Abdomen
kV	90, **120**, 140	90, **120**, 140
mAs	250, **300**, 400	**250**, 300, 400
Slice thickness	**2**, 5, 10	**2**, 5, 10

5.1.3 CBCT Acquisition

The CBCT images are obtained with the Varian Clinac iX using an on-board imaging (OBI) system (OBI v. 1.4, Varian Clinac iX, Palo Alto) (Figure 2.5). In order to simulate the patient situation (additional scatter) and based on the results obtained by Hatton et al. [21] most of the CBCT scans are carried out,

when the DP is in a container filled with water (Figure 5.3 Right). Only one CBCT scan of the HDP is carried out without water in order to investigate the effect of scanning with water.

The effect of the size of the DP and its inserts on HUs are also investigated. Therefore, CBCT scans are obtained for both HDP and PDP. HDP is scanned with the standard H&N protocol and PDP is scanned with the standard pelvis protocol (Table 5.3). In order to investigate the effect of the scan parameters on the HUs, they are varied individually for both HDP and PDP. Parameters to be varied are: kV, ms, mA and slice thickness (Table 5.4). CBCT scans are also performed using different scan protocol. The intention is to observe their effect on the HUs, when using different scan protocols. Moreover, the HDP is also scanned with the pelvis protocol. The intention is to investigate the effect of using different scan protocols for the same phantom size on the HUs.

Table 5.3: Clinical Scan Protocols in OBI v1.4 [40, 39]

CBCT Protocols	Standard Dose Head (S)	Low Dose Head (Ld)	High Quality Head (Hq)	Pelvis (p)
X-ray Voltage [kVp]	100	100	100	125
X-ray Curent [mA]	20	10	80	80
X-ray Millisecond [ms]	20	20	25	13
Bowtie filter	Full	Full	Full	Half
Reconstruction matrix [px]	200	200	200	360

Table 5.4: The investigated CBCT Scan Parameters. The standard scan settings used in clinic are highlighted [39].

Scan parameters	Standard Dose Head (S)	Pelvis (p)
X-ray Voltage [kVp]	70, 80, 90, **100**, 125	100, **125**
X-ray Curent [mA]	10, **20**, 40	63, **80**, 110
X-ray Millisecond [ms]	8, 13, **20**, 32	8, **13**, 20
Slice thickness	**2**, 5, 10	**2**, 5, 10

5.1.4 Setup of the DP

The DP was positioned by aligning markers on the container to the laser system in the treatment room (Figure 5.3).

Figure 5.3: (Left) Illustrates the set-up using the laser positioning system. Right) Illustrates the method of scanning PDP in water.

5.1.5 Construction of Calibration Curves

The obtained CT and CBCT scans are imported into TPS (Figure 4.1). Volumes of interest (VOI) are drawn on each of the material inserts. Within each VOIs, the average HUs are calculated. The REDs of the DPs tissue equivalent inserts are known in advance. Therefore, the calibration curves can be constructed by plotting the measured HUs against the REDs. The constructed calibration curves used in this study are listed below (Table 5.5). The HDP S calibration curve is used as a reference. This means that all the other constructed calibration curves will be observed in relation to this calibration curve. In this way it can be investigated, how the HUs are affected when the scan parameters are changed.

Table 5.5: Abbreviations for the constructed calibration curves. S referres to standard. The CT protocols are listed in Table 5.2 and the CBCT protocols are listed in Table 5.3

Calibration Curves	Description
CT	
HDP S	From HDP. Scans with S H&N protocol.
PDP S (ic)	From PDP (ic). Scans with S abdomen protocol.
PDP S (oc)	From PDP (oc). Scanning with S abdomen protocol.
CBCT	
HDP S	From HDP and scanned with S protocol.
HDP S -w	From HDP and scanned with S protocol, no water (-w).
HDP S-PDP	From HDP and scanned with S pelvis protocol.
HDP Ld	From HDP and scanned with Ld protocol.
HDP Hq	From HDP and scanned with Hq protocol.
PDP S (ic)	From PDP (ic) and scanned with S pelvis protocol.
PDP S (oc)	From PDP (oc) and scanned with S pelvis protocol.

5.2 Part A: Results

This chapter present the calibration curves obtained from the CT and CBCT scans when scanning the DP with different scan protocols and when varying the scan parameters (Table 5.5). The chapter only presents the curves that are affected. The rest of the calibration curves can be found in appendix A 9. The scans from which the affected calibration curves are constructed can also be found in appendix A 9.

5.2.1 CT Calibration Curves

5.2.1.1 Size of the DP and Inserts Arrangements

In this section it is investigated if the size of the DP and the inserts arrangements have an effect on the HUs.

Calibration curves are constructed from the CT scan obtained from the HDP and PDP (Figure 5.4). As the size of the DP increases, the HUs decreases for

high RED materials. For low RED materials, the HUs increase slightly as the size of the DP increases (Figure 5.5 Left). In order to investigate how the HU varies the difference (ΔHU) curves relative to the reference curve are plotted (Figure 5.5 Right). The largest ΔHU as the phantom size increases is observed for high RED materials (Figure 5.5 Right). Furthermore the ΔHU is larger for the S PDP (ic) than for the S PDP (oc) (Figure 5.5 Right). In the following only the Δ curves will be showed in order to investigate how the HUs varies, as the scan parameters are changed.

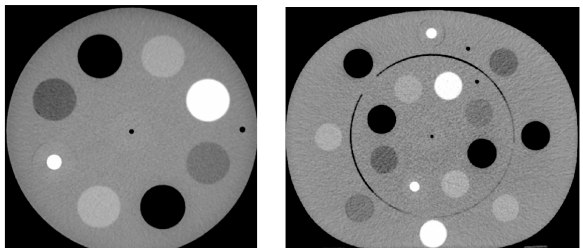

CT HDP S CT PDP S

Figure 5.4: Left) CT scan of the HDP. Right) CT scan of the PDP.

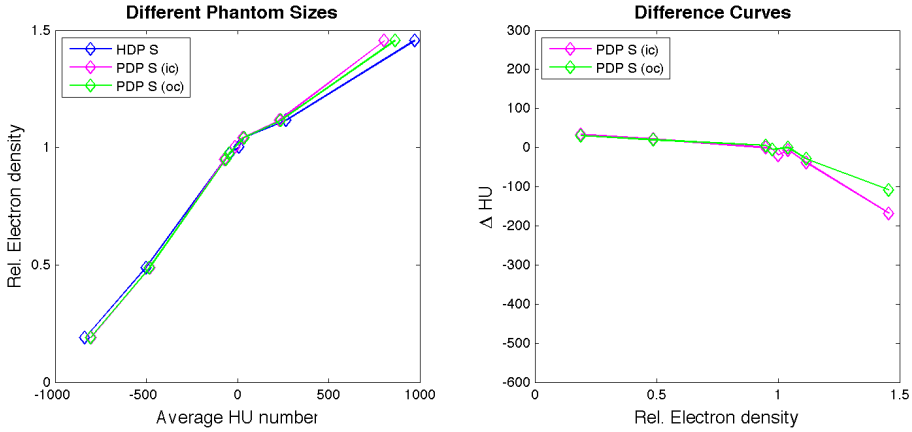

Figure 5.5: Left) Calibration curves obtained from HDP and PDP (Table 5.5). The CT scan of HDP S is used as reference (blue curve). Right) Difference curves of the calibration curves relative to the reference

5.2.1.2 Parameter Investigation

This chapter evaluates the effect on the HUs of changing the following parameters: slice thickness, mAs and kV.

No ΔHU is observed when changing the slice thickness and mAs (Figure 5.6 (a, d and g) and 5.6 (b, e and h)). The largest ΔHU is observed when changing kV (Figure 5.6 (c, f and i)). In this case the largest ΔHU is detected for high RED materials.

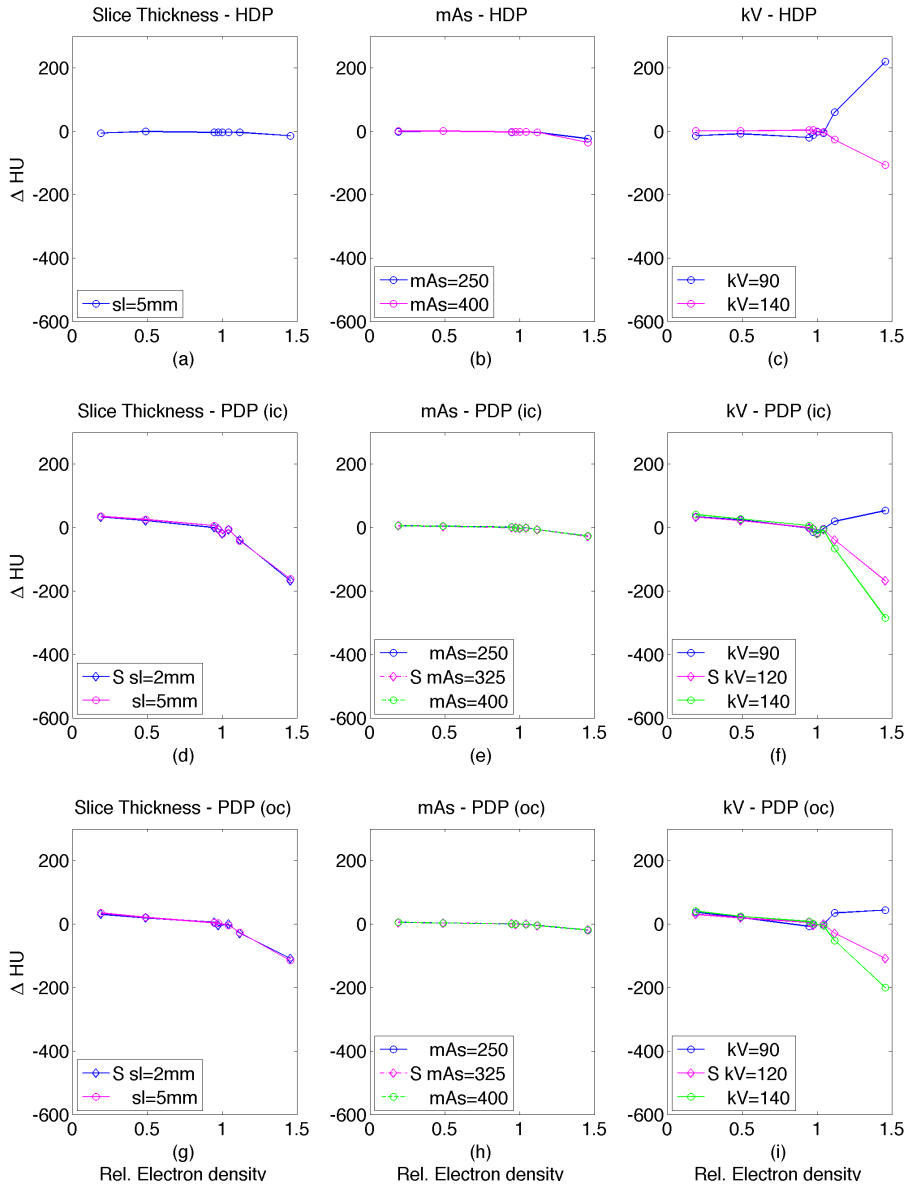

Figure 5.6: Calibration curves obtained from HDP S and PDP S when varying the parameters: slice thickness, mAs and kV. The CT calibration curve obtained from HDP S is used as reference (Table 5.5).

5.2.2 CBCT Calibration Curves

5.2.2.1 DP Scanned in Water

When scanning the DP with and without water, a ΔHU is observed for all materials (Figure 5.7). When scanning the DP with water, a smaller ΔHU compared to the reference, is detected. Furthermore, the largest ΔHU is detected for high RED materials and for low RED materials.

5.2.2.2 Size of the DP and Inserts Arrangements

The ΔHU increases, as the size of the DP increases (Figure 5.7). Furthermore, the HUs decrease for the high RED materials and increase for low RED materials as the the size of the DP increases. A ΔHU is also detected for the soft-tissue materials. The largest ΔHU are observed for low and high RED materials. Moreover, a ΔHU between the PDP S (ic) and the PDP S (oc) is observed (Figure 5.7).

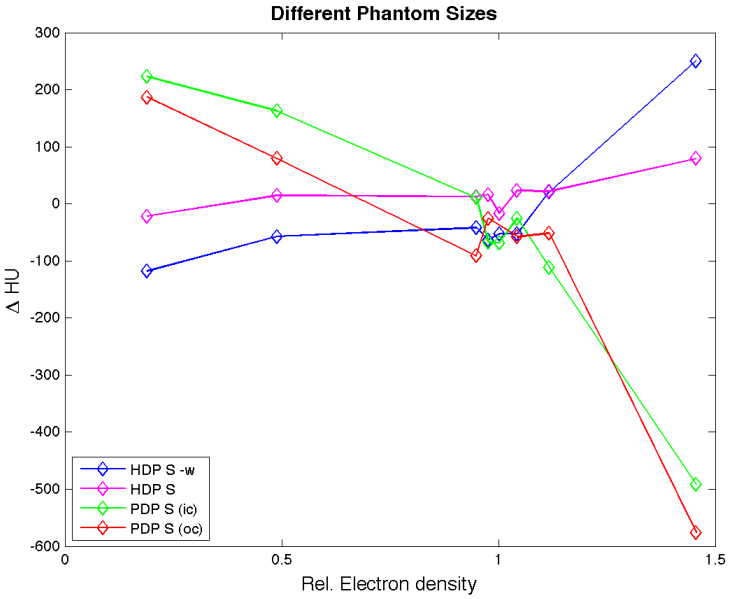

Figure 5.7: Calibration curves for HDP S with and without water and PDP (Table 5.5).

5.2.2.3 Parameter Investigation

The investigated scan parameters: slice thickness, ms, mA and kV.

For CBCT scans of the HDP and PDP, no ΔHU is observed when changing the slice thickness (Figure 5.8 (a)). When changing the parameters, ms, mA and kV a ΔHU is observed for both HDP and PDP (Figure 5.8 (b-j)). For both HDP and PDP, the largest ΔHU is detected for low and high RED materials, when changing ms, mA and kV (Figure 5.8 (b,c),(e-g) and (h-j)). This is in contrast to HDP, when changing kV where the larget ΔHU is detected for soft-tissue materials (Figure 5.8 (d)). It is further noticed that for kV $>$ 70 the ΔHU decreases. Also it is observed, that there are differences in ΔHU between the PDP (ic) and the PDP (oc) when changing the parameters (Figure 5.8 (e-j).

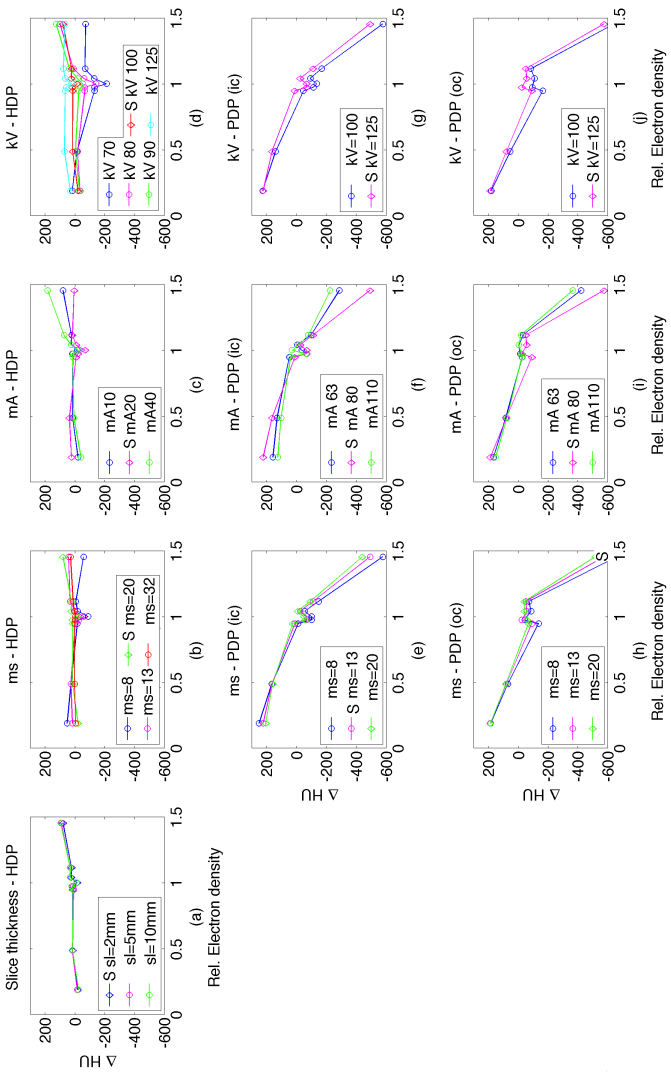

Figure 5.8: Calibration curves obtained from the CBCT scans of the HDP and PDP when varying the parameters: slice thickness, mAs and kV. The CT scan of the HDP S is used as a reference (Table 5.5). The curves constructed with standard scan parameteres are marked with diamonds.

5.2.2.4 Investigation of Different CBCT Protocols

The HDP is scanned with different CBCT protocols, S, Hq and Ld (Table 5.3).

Scanning with different CBCT protocols results in ΔHUs (Figure 5.9). The largest ΔHU is observed for low and high RED materials, when scanning HDP with Hq protocol.

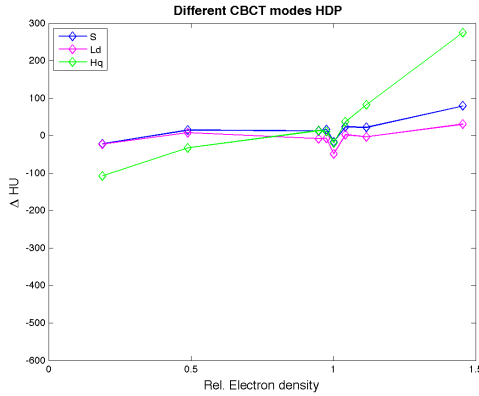

Figure 5.9: Calibration curves when scanning with different CBCT modes, S, Ld and Hq (Table 5.5).

5.2.2.5 Different scan Protocols for the same Patient

It is observed, that when scanning the HDP with different protocols, the H&N protocol and Pelvis protocol, effect the HUs (Figure 5.10). The largest ΔHU is observed for the high RED materials, when comparing the two calibration curves.

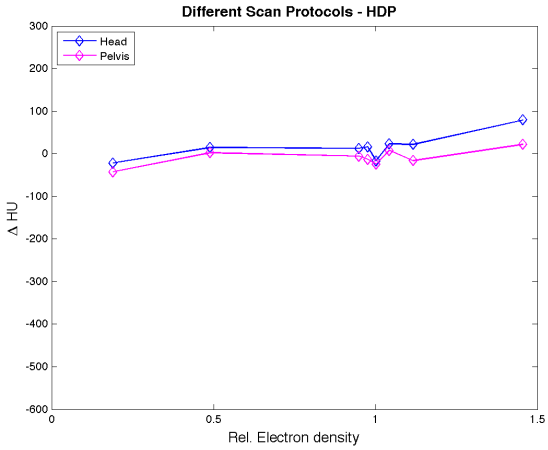

Figure 5.10: Calibration curves when scanning HDP with different protocols (Table 5.5).

5.3 Part A: Discussion

A smaller ΔHU compared to the reference was found, when scanning the DP in water (DP with scatter) compared to without water (DP in air) for all materials. Hatton et al. [21] found a maximum dose difference of 2-3% between CT and CBCT using calibration curves obtained from the DP with scatter. This was in contrast to the observed 15% dose difference when calculating the dose distribution from CBCT using the calibration curve when scanning the DP in air. Based on their results a least deviation between the CBCT- and CT- based dose distribution using the calibration curve obtained from CIRS with scatter would be expected. Compared to the study Hatton et al. [21] our result is based on ΔHU. Although it is reasonable to assume, that these ΔHU would also lead to dose distribution differences when scanning with or without water.

The HUs for both CT and CBCT are affected by the DP size and insert arrangement. This is probably due to the increased amount of detected scatter, as the size of the DP increases which affects the accuracy of the HUs [45, 34]. This explains the observed ΔHU for PDP S (ic) and PDP S (oc). However these observations were more notable for the CBCT scans (Figure 5.5 and 5.7). The increase in ΔHU, as the DP size increase were confirmed by Rong et al. [34] and Hatton et al. [21]. The observed ΔHU between PDP S (ic) and PDP S (oc) were confirmed by Rong et al. [34]. These observations suggest the use of different calibration curves for H&N patients and pelvis patients, especially for

CBCT.

For CT and especially CBCT the HUs obtained from both the HDP and PDP are mainly effected by changing kV (Figure 5.6 (c, f, i) and 5.8 (d, g and j).This was expected since varying voltage changes the energy of the photons and thereby the HUs. Higher photon energy results in less attentuation of the x-rays and thereby a decrease in HU. The opposite is observed for low energy photons.

The effect in varying the parameters mA and ms on the ΔHUs are evaluated. A change of these parameters is observed when scanning with different CBCT scan protocols and when investigating the scan parameters seperately. Therefore these observations will be discussed together. For CBCT, it was detected, that mA and ms have an effect on the ΔHUs, but mostly for low- and high- RED materials (Figure 5.8 (b-c, e-f and h-i) and 5.9). The tube current and milisecond are proportional with the number of generated photons and do not affect the ΔHU. This is in agreement with the observation found by Y. Rong et al. [34]. The effect observed in our study is smaller compared to what was observed when changing voltage. The observations from our study are based on only one scan and the variation in HUs between scans are unknown. These ΔHU are contributed to a combination of scatter and HU variation between scans.

ΔHUs were observed, when scanning HDP with H&N protocol and Pelvis protocol (Figure 5.10). This is probably due to the higher voltage used in the pelvis protocol. A future research project must be carried out in order to investigate if a protocol-specific calibration curve is needed for the dose calculation on CBCT.

5.4 Part A: Conclusion

This study investigated the effect of using several parameters effect the HUs. It was found that CBCT is more easily affected than CT when changing the parameters, especially the kV parameter. ΔHUs have been observed when scanning with different CBCT scan protocols. The efffect of the size of the DP and its inserts on the HUs was investigated. From this it was found, that the HUs from CBCT were affected the most by the phantom size and insert arrangements, but CT was also affeceted. The need for using site- and protocol- specific calibration curves for dose calculation depends on how large an effect the calibration curve has on the dose calculation. The former will be investigated in the clinical study.

Chapter 6

Part B: Phantom study

A phantom study is performed with the purpose of investigating the use of different scan protocols and calibration curves for the CBCT based dose calculations (Figure 6.1,4.1). The intention is to determine a scan protocol and calibration curve which will results in a CBCT based dose distribution similar to the CT based dose distribution.

6.1 Part B: Materials and Method

Illustration of the method used in this thesis (Figure 6.1,4.1).

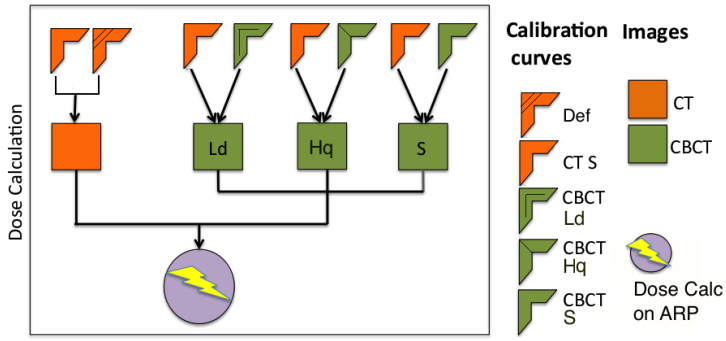

Figure 6.1: A CT and several CBCT scans are obtained from Alderson (Figure 6.2). The CT scan is obtained with standard H&N scan protocol (Table 5.2). The CT based dose calculation is calculated using the CTS calibration curve, which referres to the curve obtained from the CT scan with standard scan parameters. Also, the Def. calibration curve available in the TPS is used for the CT dose calculation. The intention is to compare with the CT based dose calculation using the measured CT calibration curve. The calculated dose distributions on CBCT will be compared to this CT based dose distribution. The CBCT scans are obtained with different CBCT protocols, low dose head (LD), high quality head (Hq) and standard (S) (Table 5.3). The intention is to find the most appropriate scan protocol for the CBCT based dose calculation. The dose calculation on CBCT is calculated using some of the computed calibration curves from the previous study (Part A). These calibration curves are obtained from the corresponding CBCT scan protocols. Furthermore, the CBCT based dose calculation is calculated using the CTS calibration curve. The CBCT based dose calculations are compared with the CT based dose calculation, which is used as a reference. The intention is to investigate, whether the CBCT calibration curves are more accurate than the CT calibration curve for dose calculation on CBCT. The calibration curves used for this phantom study is selected among the calibration curves obtained in Part A (Chapter 5)

6.1.1 Data Specification

For this study the head part of the Alderson RANDO phantom is used (Figure 6.2) [4]. It is an anthropomorfic phantom made of tissue-equivalent materials. In the following this phantom will be referred to as ARP.

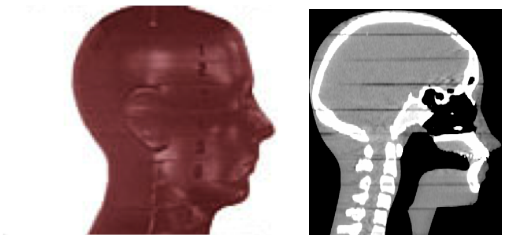

Figure 6.2: a) ARP, adapted from [4], b) Reconstruction of ARP.

The CT scan includes a structure set consisting of a target volume and OARs (Figure 6.3). The CT also has an approved IMRT plan available.

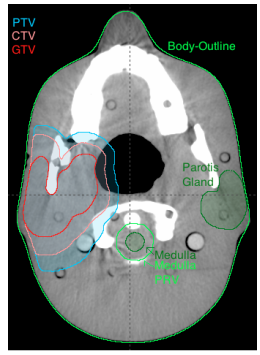

Figure 6.3: ARP with a structure set.

6.1.2 Data Processing

The data are extracted from the clinic database and is further processed on a computer in a ”clinical stand alone” system (Training - box) where TPS is also available.

6.1.2.1 Image Registration

After the import of the CT and CBCT images, a 3D/3D registration is carried out in TPS (Figure 6.4). Firstly the images are manually matched mainly by aligning the bone structures. Then an automatic rigid registration is carried out in order to finely adjust the registration. Rigid registration is a geometrical match based on translation and rotation. It is performed within a predefined volume of interest (VOI) and uses a similarity measure to determine how well the images match. Rigid registration is used to adjust for different patient positions between the scans [31, 27].

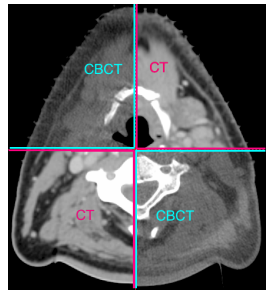

Figure 6.4: H&N patient: The match of CT and CBCT after registration is illustrated using a split window. This patient is used later on in the clinical study (Part C).

6.1.2.2 Procedure for Dose Calculation

After image registration, a 3D dose distribution based on CT and CBCT is calculated for ARP. Before the dose is calculated from CBCT, the structure set and IMRT plan from CT is transferred to CBCT. The calculated dose distribution is based on the Anisotropic Analytical Algorithm (AAA) and is carried out in TPS. In order to evaluate the use of CBCT for dose calculation, the same IMRT plan and MU as for CT is used. Within the TPS, multiple calibration curves can be stored [40]. It also, permits the user to select a specific calibration curve before dose calculation. This provides the opportunity of comparing dose distributions calculated with different calibration curves for the same patient.

6.1.2.3 Abbreviations for Dose Calculation

Abbreviations for the different calibration curves selected for the dose calculations are listed in Table 6.1. This table is used in both Part A and B.

The abbreviation consist of two terms: The first term denotes the scan upon wich the calculation of the dose distribution is based. The second term indicated by an underscore denotes the use of the calibration curve for dose calculation. For instance, CTS_Def denotes the dose distribution calculated on CTS with the use of the Def. calibration curve available in TPS (Eclipse). Furthermore CTS represent the CT scan obtained with the standard (S) H&N scan protocol (Table 5.2). Another example, CTS_CTS denotes the dose distribution calculated on CTS with the use of the calibration curve obtained from CTS. The dose calculated on CB S, Hq and Ld present the CBCT scans obtained with standard dose head, low dose head and high quality dose head protocols respectively (Table 5.3). A last example is, CBp_poc which represent the dose calculation on CBp using the calibration curves obtained from the PDP (oc). CBp present the dose calculated on CBCT of PDP.

Table 6.1: Abbreviation for the Dose Calculations on ARP and Patients (Section 7)

Dose Calculation	First term	Second term
H&N		
CTS_Def	Dose calc on CTS	Calib curve from TPS (Eclipse)
CTp_Def	Dose calc on CTp	Calib curve from TPS (Eclipse)
CTp_CTpoc	Dose calc on CTp	Calib curve from CT of PDP (oc)
CTS_CTS	Dose calc on CTS	Calib curve from CTS
CBS_Def	Dose calc on CBS	Calib curve from TPS (Eclipse)
CBS_CTS	Dose calc on CBS	Calib curve from CTS
CBS_CBS	Dose calc on CBS	Calib curve from CBS
CBHq_CTS	Dose calc on CBHq	Calib curve from CTS
CBHq_CBHq	Dose calc on CBHq	Calib curve from CBHq
CBLd_CTS	Dose calc on CBLd	Calib curve from CTS
CBLd_CBLd	Dose calc on CBLd	Calib curve from CBLd
Cervix		
CBS_CBpoc	Dose calc on CBS	Calib curve from CB of PDP (oc)
CTp_CTpoc	Dose calc on CTp	Calib curve from CT of PDP (oc)
CBp_CTpoc	Dose calc on CBS	Calib curve from CB of PDP (oc)
CBp_CBpoc	Dose calc on CBp	Calib curve from CB of PDP (oc)
CBp_CBpic	Dose calc on CBp	Calib curve from CB of PDP (ic)

6.2 Part B: Evaluation

6.2.1 Dose Volume Histograms - DVH

The CT- and CBCT- based dose distribution are evaluated by comparing DVHs and DVH points for the targets volumes and OARs. The evaluated DVH points are the ones used in the clinic at Herlev Hospital for H&N patients. The DVH points for the PTV was presented previously in section 2.10.

For the OARs, the DVH points to be compared are based on the recommendation given by the clinical guidelines from DAHANCA (Figure 6.2) [5].

Table 6.2: DVH points for the OARs to be compared for ARP.

Structure	**Description**
Medulla	The maximum dose, D_{max}
Medulla PRV	The maximum dose, D_{max}
Parotis	The mean dose, D_{mean}

As the right parotis is within PTV and receives full dose only the left parotis will be evaluated in this study. Only the left parotis in this study will be evaluated. This is due to, that the right parotis in ARP is within PTV and receives full dose.

Furthermore, the standard deviation (STD) of the dose distribution for PTV and OARs are evaluated. STD is a measure which describes to what extend the dose distribution deviates from the mean dose. The calculated STD for the dose distribution within a structure will be referred to as STD in the following.

For the purpose of comparison the percentual dose differences compared to CT are calculated for the DVH points when using different calibration curves. They will also be compared to percentual dose differences observed in similar studies.

6.3 Part B: Results

Details described in this section are listed in tables found in the appendix (Table 10.1, 10.2 and 10.3).

PTV It is observed that the DVH for CTS_CTS contributes with a larger volume for a given dose than CTS_Def (Figure 6.5). Comparing DVH points, a maximum dose difference of 0.6% is detected.

The DVHs for CBLd_CBLd and CBLd_CTS contribute with the smallest relative volume for a given dose compared to CTS_CTS.

Comparing the DVHs for CBHq_CBHq and CBHq_CTS it is observed that both are close to CTS_CTS, but CBHq_CBHq is the closest.

The figure shows, that the DVHs for CBS_CBS and CBS_CTS are almost identical and that the DVHs are most similar to the CTS_CTS. When comparing DVH points a 0.3% of maximum dose difference is observed between CTS_CTS and CBS_CBS and CBS_CTS respectively.

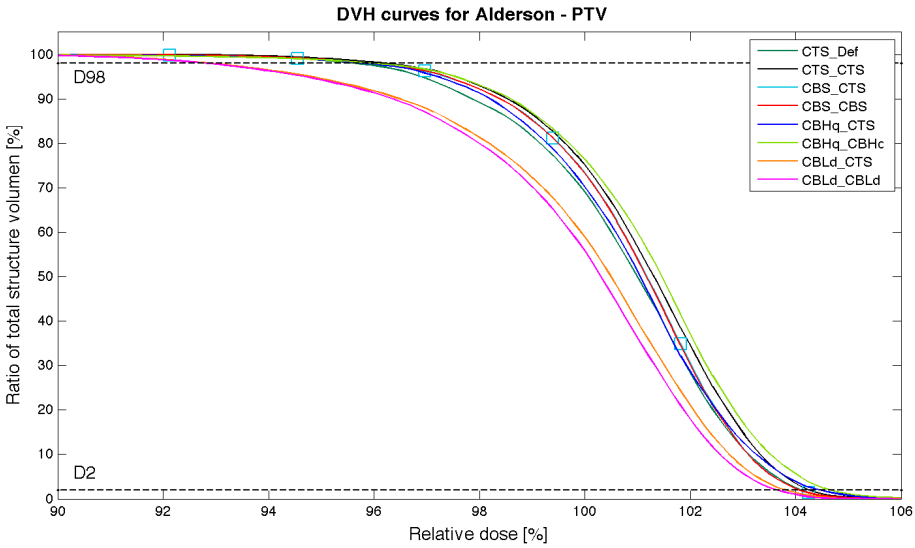

Figure 6.5: ARP: DVHs for PTV when the dose distributions for CT and CBCT are calculated using different calibration curves (Abbreviations Table 6.1). The investigated DVH points are illustrated with dotted horisontal lines.

OARs

By visual inspection of the DVHs for medulla using different calibration curves, almost no difference between the DVHs is detected (Figure 6.6). In order to investigate how the HUs are affected using different scan protocols, DVH points for the OARs are compared. The use of the CBLd protocol have showed to result in a dose distribution their deviate the most from CTS_CTS. An exception is detected for medulla, where the use of CBHq protocol results in the highest dose deviation. Using the CBHq protocol a 7.7% maximum dose difference compared to CTS_CTS was observed.

For all the OARs it is noticeable, that the use of CBS protocol yields results which are most similar to the results of CTS_CTS. In this case a 3.5% maximum dose difference is observed for parotis. For the volume of parotis a high dose STDs are observed with a maximum STD of 13.9 Gy.

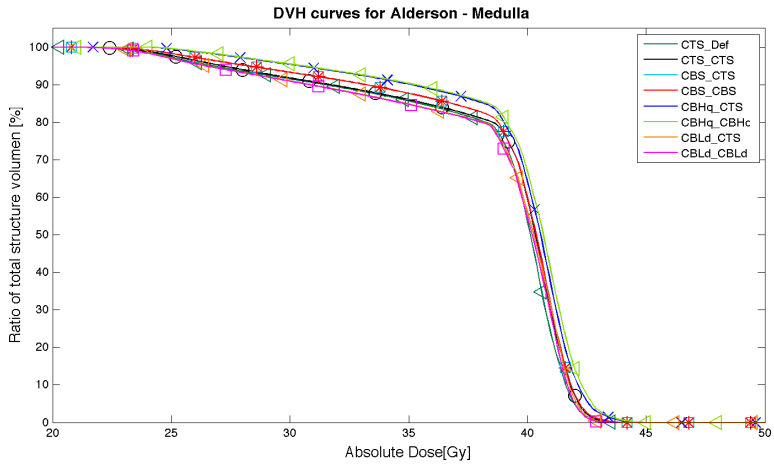

Figure 6.6: ARP: DVHs for medulla when the dose distributions for CT and CBCT are calculated by using different calibration curves.

6.4 Part B: Discussion

The study shows a difference between the DVHs for CTS_CTS and CTS_Def. From this it can be concluded, that the use of a measured CT calibration curve compared to the one available in TPS affect the calculated dose distribution. The observed 0.6% maximum dose difference does not have clinical relevance.

With the use of the CBLd protocol, the dose distribution least similar to the CTS_CTS is achieved. Since the intention of this study is to achieve a CBCT based dose distribution similar to the dose distribution calculated on CT, the use of the CBLd protocol is discouraged.

For PTV, a dose distribution similar to CTS_CTS was shown for both CBS_CBS and CBHq_CBHq. It cannot be determined which protocol is more appropriate than the other. Using CBHq protocol a 7.7% maximum dose difference compared to CTS_CTS was observed for the OARs. Using this protocol the patient receives a higher dose due to the higher tube current compared to using CBS protocol. Therefore, this study does not recommend the use of the CBHq protocol.

Previously, it was concluded that the use of CBLd and CBHq protocols are not recommended. It is left to evaluate the CBS protocol:
For PTV a maximum dose distribution difference was found to be 0.3% when comparing CBS_CBS to CTS_CTS. For the OARs a maximum dose difference was found to be 3.5% for parotis. This 3.5% difference is negligible seen in the light of the observed high dose STD. A similar phantom study by Y. Rong et al. [34] found a high agreement between the CBCT and CT based dose distributions. Y. Rong et al. found DVH differences for PTV and OARs to be less than 1% and suggest that CBCT can be used for dose calculation. From their study as well as our study it is recommended that CBCT can be used for dose calculation using the CBS protocol.

It is now evaluated which calibration curve is the most appropriate:
It was examined, if it is nessesary to use the CBS calibration curve compared to the CTS calibration curve for the CBCT based dose calculation. The results show that using the CBHq calibration curve results in a dose distribution closer to that of the CTS_CTS than using the CTS calibration curve. This behaviour is expected, since a HU value in CBCT will be assigned a different RED value using a CT calibration curve compared to a CBCT calibration curve. This is due to an off-set between the calibration curves. These observations are not detected when using the CBS calibration curve. Both calibration curves will

therefore be tested in the clinical study.

6.5 Part B: Conclusion

It can be concluded that the observed dose difference on CT using the measured CT calibration curve compared to the Def. calibration curve have no clinical relevance. The CBS protocol is concluded to be the most appropriate for the CBCT based dose calculation. A further investigation is needed in order to evaluate which calibration curve to use. This further evaluation will be examined in the clinical study.

Chapter 7

Part C
Clinical Study

This study is performed with the intention of evaluating the results from the phantom study (Part B, Chapter 6) in a clinical perspective (Figure 4.1).

7.1 Part C: Materials and Method

7.1.1 Patient Specification

The data used for this study is an H&N cancer patient and a cervix patient (Table 7.1). Patients whose CT and CBCT are alike are selected for this study. The H&N patient is treated with IMRT and the cervix patient is treated with RA. Due to the limited FOV with CBCT some informations are lost on the edges of the CBCT images. This may cause errors in the CBCT based dose calculation if the delineated structures copied from the planning CT are not included in the CBCT. Therefore the patients are selected in order to minimize this problem.

Table 7.1: Data used in this thesis

Patient	Gender/age	Specifications	Dose [Gy]	Days between the CT and CBCT scans
H&N	M/48	Oropharynx	68	7
Cervix	F/63	Cervix	60	1

The data include a CT and a CBCT scan obtained with standard scan parameters (Table 5.2 and 5.3). The CT scans also include a structure set containing a body outline and delineated structures for targets and OARs (Figure 7.1). The data processing is as described in the phantom study (Chapter 6).

7.1.2 Calibration Curves used for Dose Calculation

The procedure for dose calculation is described in the previous chapter (Chapter 6, Table 6.1).

7.1.2.1 H&N

The CT based dose distribution for PTV and OARs are calculated using the measured CTS calibration curve and the Def. calibration curve available in TPS (Eclipse). The purpose is to investigate, which effect the measured CT calibration curve compared to the Def. calibration curve has on the CT based dose distribution.

The dose distribution on CBCT is calculated using the CBS calibration curve and CTS calibration curve. The intention is to investigate which calibration curve is the most appropriate for the dose calculation on CBCT. For clinical comparison the Def. calibration curve is used for the dose calculation on CBCT for PTV.

The CBpoc calibration curve and CBpic calibration curve are used for the dose calculation on CBCT. The intention is to investigate if using different calibration curves can affect the dose calculation on CBCT and if a site-specific calibration curve for different patient groups are needed. Also, it is investigated if the use of these two calibration curves yield different DVHs.

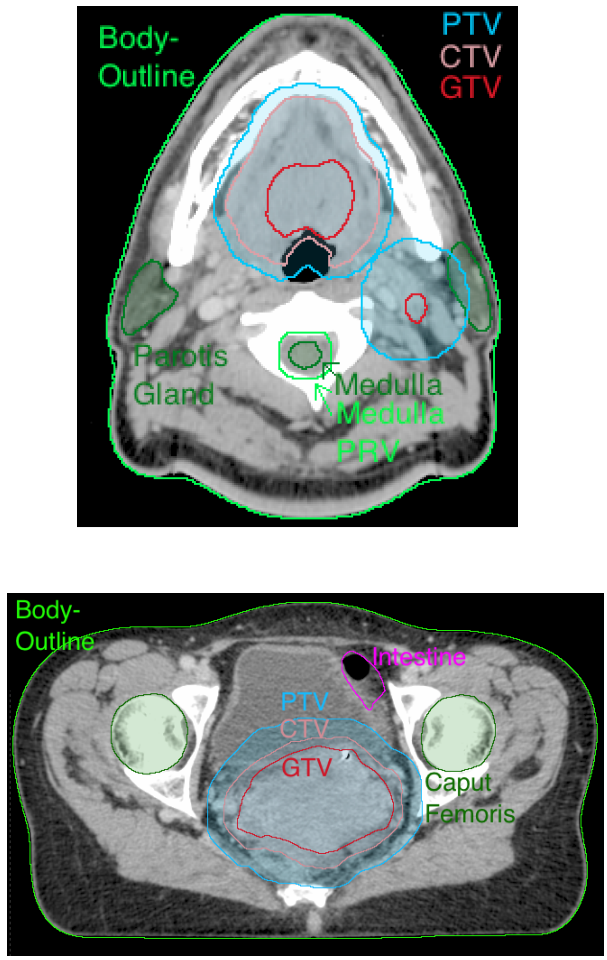

Figure 7.1: A slice of the patients used in this thesis (Table 7.1). Left) Reconstruction of the H&N cancer patient with a structure set. Right) Reconstruction of the cervix cancer patient with a structure set.

.

7.1.2.2 Cervix

The CT based dose distribution is calculated using the calibration curves, CTpoc and Def. The purpose is as with the H&N patient to investigate the effect of using a measured CT calibration curve compared to the one available in TPS. CTp_CTpoc is used as a reference in this section (Table 6.1).

The CBCT based dose calculation is computed using a CTpoc calibration curve and a CBpoc calibration curve (Table 6.1). This is done in order to determine which calibration curve achieves a CBCT based dose distribution most similar to CT.

7.1.3 Part C: Evaluation

7.1.3.1 H&N

Evaluation of the H&N cancer patient is as described for the ARP (Chapter 6, Section 6.2).

7.1.3.2 Cervix

The same DVH points for PTV are evaluated as for the ARP (Chapter 6, Section 6.2).

For the OARs, the DVH points to be compared are based on the local clinical guidelines used in the clinic at Herlev Hospital (Table 7.2).

Table 7.2: DVH points to be compared for the OARs for the cervix patient.

Structure	Description
Femur	The maximum dose, D_{max}
Intestine	The volume which receives 45 Gy, $V_{45\ Gy}$

7.2 Part C: H&N

The results described in this section are listed in tables found in appendix B (Table: 10.4), 10.5 and 10.6).

7.2.1 Results

PTV
Different DVHs are observed for CTS_CTS and CTS_Def (Figure 7.2). A maximum dose difference of 1.7% is evident when DVH points are compared.

It is observed that the DVHs for CT and CBCT using different calibration curves are almost shifted versions of each other.

The DVHs for CBS_CBS and CBS_CTS are almost equal and are closest to CTS_CTS. A comparison of DVH points yields a 0.3% maximum dose difference between CBS_CBS and CTS_CTS.

OARs
The DVHs obtained using different calibration curves contribute with the same volume regardless of the given dose (Figure 7.3). A maximum dose difference of 1.1% is observed for parotis.

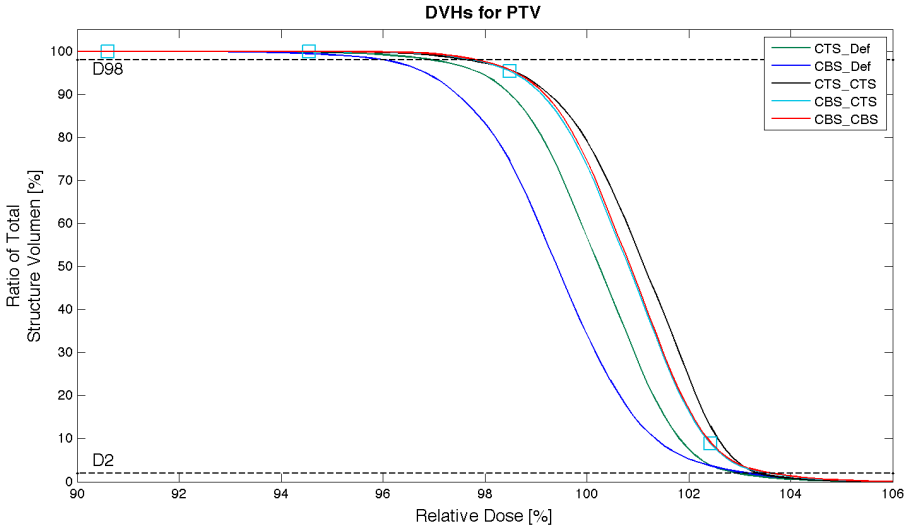

Figure 7.2: H&N: DVHs for PTV when the dose distributions for CT and CBCT are calculated using different calibration curves. The investigated DVH points are illustrated with dotted horisontal lines. Abbreviations (Table 6.1)

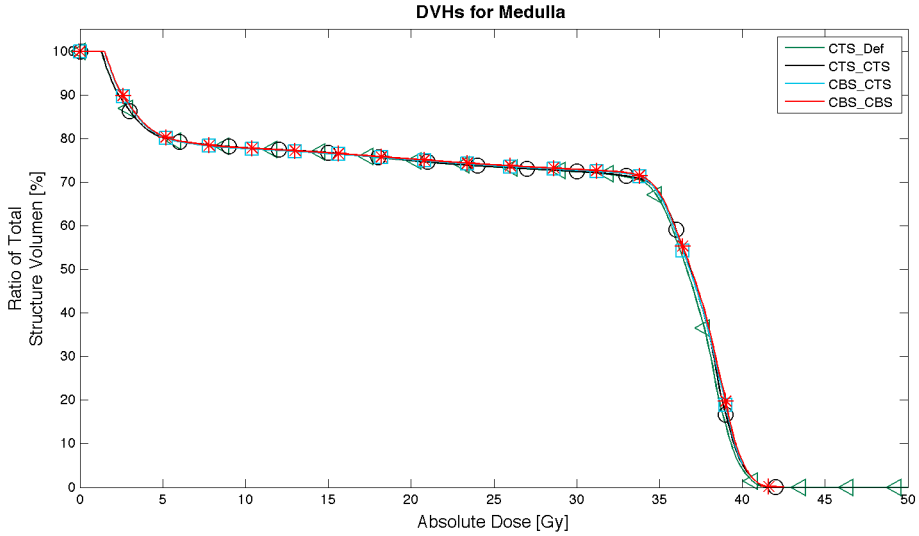

Figure 7.3: H&N: DVHs for medulla when the dose distributions for CT and CBCT are calculated by using different calibration curves. Abbreviations (Table 6.1)

7.2.2 Discussion

For PTV it was observed that the DVHs for CT and CBCT using different calibration curves are almost shifted versions of each other (Figure 7.2). This is due to the different calibration curves used for the dose calculation.

When comparing DVH points a maximum dose difference of 1.7% is found between using the measured calibration curves and the Def. calibration curve. Similar studies which evaluates the use of CBCT for dose calculation accept a dose difference between CT and CBCT within 2% [6, 34].

For PTV, the DVHs for CBS_CBS and CBS_CTS are almost equal and closest to CTS_CTS and a 0.3% dose distribution difference is detected. The same is evident from the ARP study (Part B) where the evaluation is confirmed by a similar study by Y. Rong et al. [34]. The OARs showed a maximum dose difference between CT and CBCT of 1.1%. The detected percentual dose differences for PTV and OARs are both within the 2% found in similar studies [6, 34]. The findings of the above mentioned studies, as well as the results of this project, suggest that CBCT can be used for dose calculation seen in a clinical perspective. This outcome was expected, since the used calibration curves were the same.

This clinical study was not able to determine whether the CBS calibration curve or the CTS calibration curve was the most appropriate for the dose calculation on CBCT.

In order to clarify this, a future research project must include an investigation of the 3D dose distribution in more patients and other regions of the ARP.

7.2.3 Conclusion

This clinical study of the H&N patient concludes, that the observed dose difference between using the Def. calibration curve compared to the CTS calibration curve does not have clinical relevance. It is concluded that CBCT can be used for dose calculation using the CBS protocol. However, it is concluded that an investigation of more patients and other ARP regions regarding the 3D dose distribution is needed to determine whether the CBS calibration curve or the CTS calibration curve is more appropriate for the CBCT based dose calculation.

7.3 Part C: Cervix

The results described in this section are listed in tables in appendix B (Table: 10.7, 10.8 and 10.9).

7.3.1 Results

PTV
Different DVHs are observed for CTp_CTpoc and CTp_Def (Figure 7.4). A maximum dose difference of 7.5% is evident when DVH points are compared.

When comparing DVHs for CBp_CTpoc and CBp_CBpoc it is noticed, that both are similar to CTp_CTpoc. The results show a 6.2% maximum dose difference between using CBp protocol compared to the CTp protocol.

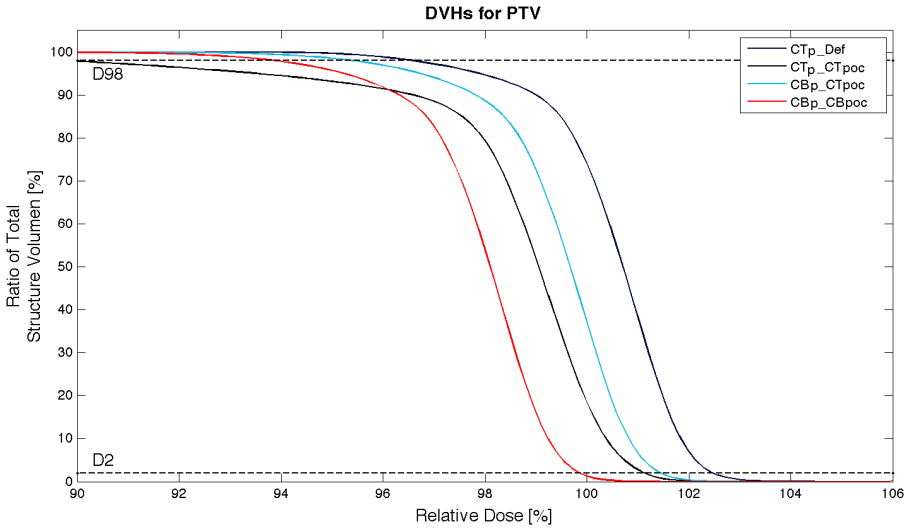

Figure 7.4: Cervix: DVHs for PTV. Dose distributions for CT and CBCT are calculated using different calibration curves. The investigated DVH points are visualised wih dotted horisontal lines. Abbreviations (Table 6.1)

OARs
A 13.2% maximum dose difference is detected for intestine. There is no clear pattern as to whether the CBCT based dose calculation is closer to CTp_CTpoc or to CTp_Def. Also, no pattern has been detected as to whether the use of the CBpoc calibration curve or the CTpoc calibration curve achieves a better CBCT dose distribution.

7.3.2 Discussion

When comparing DVH points, a 6.2% maximum dose difference was observed using CBp protocol compared to CTp protocol. For the OARs, a 13.2% maximum dose difference was detected. This is in contrast to the 2% maximum dose difference between CBCT and CT observed by Y. Rong et al.[34] and Y. Yang [45]. In our study the dose distribution is calculated on a patient, whereas in their studies the dose distributions are calculated on the PDP. This partly explains the higher dose difference observed in our study.

The results showed contradicting indications whether the CBCT based dose calculation is closer to CTp_CTpoc or to CTp_Def. Also, whether the use of the CBpoc calibration curve or the CTpoc calibration curve achieves a better CBCT based dose distribution. DVH points for the cervix patient shows higher dose differences compared to the DVH points for the H&N patient. For instance a 7.5% versus a 1.7% maximum dose distribution difference between the Def. and measured CT calibration curve for the cervix patient and the H&N patient respectively were detected.

These observations suggest that further studies to investigate the use of CBCT dose calculation on pelvis patients is required.

7.3.3 Conclusion

It is concluded, that further investigation is required in order to investigate if CBCT based dose calculation is accurate enough for pelvis patients.

7.4 Part C: Different Calibration Curves for the same Patient

7.4.1 Results

PTV
DVHs for CBS_CBS resemble the CTS_CTS better than the DVHs of CBS_CBpoc and CBS_CBpic (Figure 7.5). A 2.2% maximum dose error is found between using the CBS calibration curve compared to using the CBpos calibration curve or the CBpis calibration curve respectively.

Similar DVHs are showed for CBS_CBpoc and CBS_CBpic.

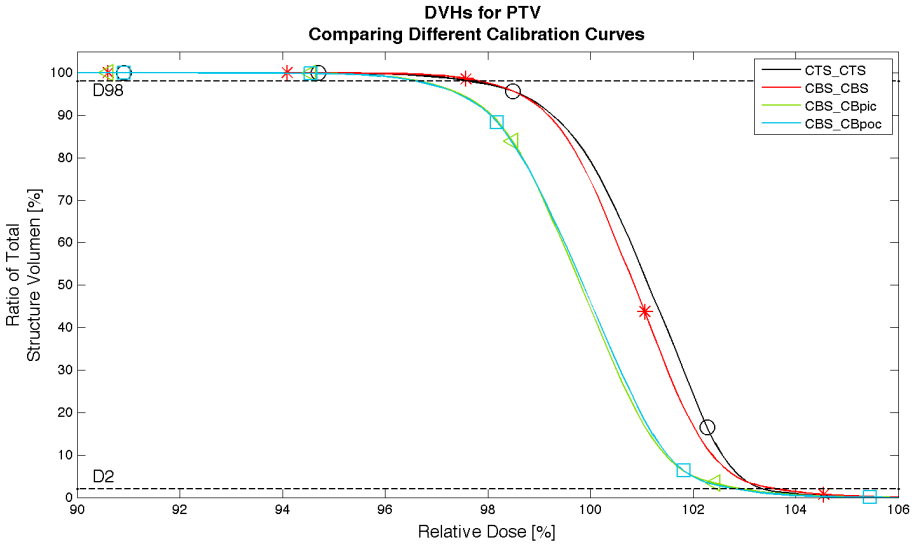

Figure 7.5: H&N: DVHs for PTV. Dose distributions for CT and CBCT are calculated using different calibration curves. The investigated DVH points are visualised wih dotted horisontal lines. Abbreviations (Table 6.1)

OARs
The same pattern is evident for the medulla DVHs. CBS_CBS better resembles the CTS_CTS than CBS_CBpoc or CBS_CBpic does (Figure 7.6). A 4.2% maximum dose error is found between using the CBS calibration curve compared to

using the CBpos calibration curve or the CBpis calibration curve.

As is the case for PTV, similar DVHs are observed for CBS_CBpoc and CBS_CBpic.

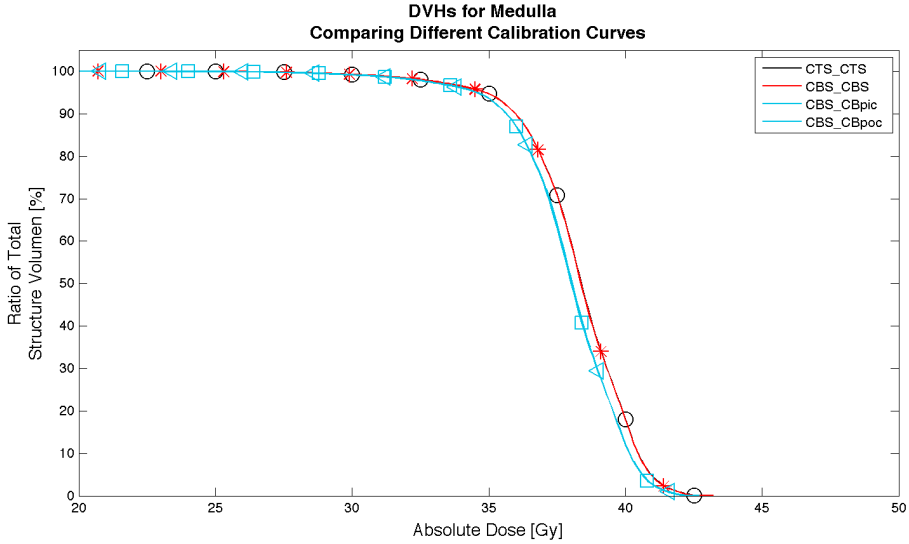

Figure 7.6: H&N: DVHs for medulla. Dose distributions for CT and CBCT are calculated using different calibration curves. Abbreviations (Table 6.1)

7.4.2 Discussion

The resemblance between CBS_CBS and CTS_CTS are discussed previously (Subsection 7.2.2).

The findings suggest that site-specific calibration curves for different patient groups are required in order to achieve a dose calculation on CBCT which resembles the CT based dose distribution the most. This is confirmed by other similar studies [21, 33, 34]. The use of a site-specific calibration curve for CBCT resulted in a dose difference between CT and CBCT within 2%. The same is found by Y. Rong et al. [34] and A. Richter et al.[33].

The DVHs for CBS_CBpoc and CBS_CBpic showed similar DVHs. In Part A it was shown that the insert arrangement affect the HUs (Figure 5.7) (Chapter

5). HWne using these two calibration curves an approximate maximum ΔHU of 100 was noticed. The findings suggest that the ΔHU of 100 in this case does not affect the calculated dose distribution on CBCT.

For the H&N patien a 4.2% maximum dose error was found by our study using the pelvis calibration curve for the dose calculation on CBCT instead of H&N calibration curve. Similar results were obtained by Y. Rong et al. [34]. Y. Rong et al. observed a 3% dose error or higher if the H&N calibration curve is used for all other body regions. This confirms the importance of using a site-specific calibration curve for different patient groups.

7.4.3 Conclusion

It is concluded that a site-specific calibration curve for different patient groups results in a dose calculation on CBCT best resembles the CT. If the pelvis calibration curve is used for dose calculation on other body parts, a 4.2% dose error can occur.

Chapter 8

Final Conclusion

The aim of this study was to investigate, if CBCT could be used for dose calculation in order to predict and assess the dose delivered to the patient a daily basis.

The presented results derive from scanning the DP, where calibration curves were established for various parameters and DP configurations. It was found that CBCT was affected the most, especially for the kV parameter. Also, it was evident that the DP size and its configurations affect the HUs. It was found that the ΔHUs increased as the DP size increased.

For the ARP the dose calculations on CBCT were calculated using the calibration curves obtained from the different scan protocols. Our study recommended the use of the CBS protocol for the dose calculation on CBCT. Furthermore, the dose calculation on CBCT was calculated using the CT calibration curve. This was done with the purpose of investigating if the CBCT calibration curve is more accurate for the CBCT based dose calculation compared to using the CT calibration curve. It was concluded that further investigation was needed in order to evaluate which calibration curve to use. This investigation was carried out in a clinical study.

The clinical study included an H&N patient and a cervix patient. The results showed that CBCT could be used for dose calculation for the H&N patient, but

it also showed that further investigation for the pelvis patients is required. The following results relate to the H&N patient. It was concluded, that the detected ΔHU between the CT calibration curve and the Def. calibration curve has no clinical relevance. Also, it was concluded that a site-specific calibration curve was needed in order to achieve a dose calculation on CBCT similar to that of CT. Future research should focus on clarifying whether a protocol-specific calibration curve is needed based on the detected ΔHU between using different scan protocols for the same patient.

Chapter 9

Appendix A

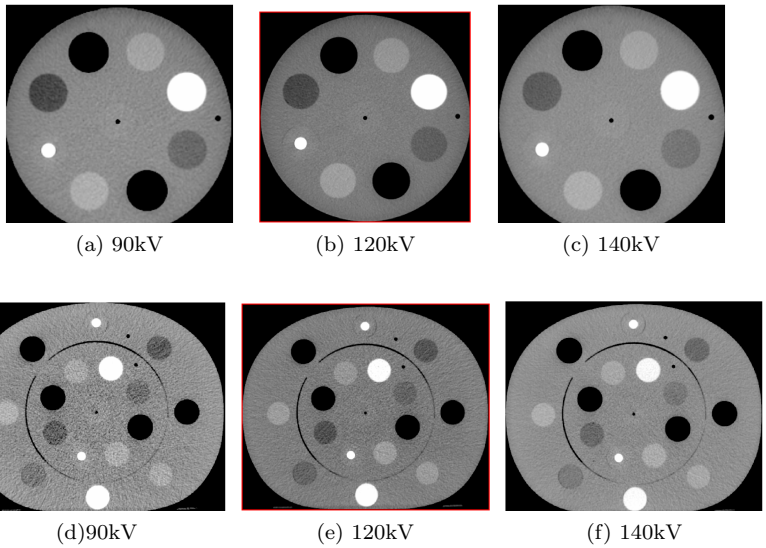

(a) 90kV (b) 120kV (c) 140kV

(d)90kV (e) 120kV (f) 140kV

Figure 9.1: CT images of the HDP (a-c) and PDP (d-f) varying kV. The image obtained with standard parameters is highlighted with a squared red box.

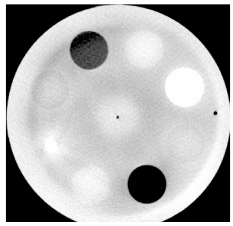

CBCT S HDP without water

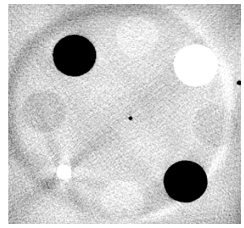

CBCT S HDP with water

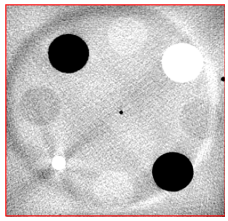

(a) Slice = 2mm

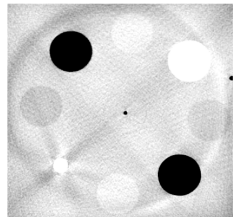

(b) Slice = 5mm

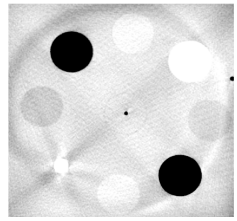

(c) Slice = 10mm

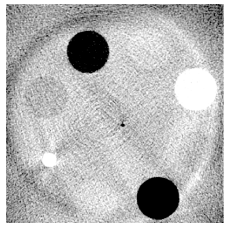

(e) 8ms

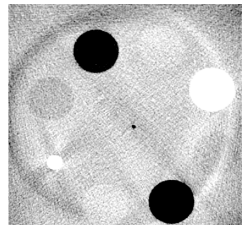

(f) 13ms

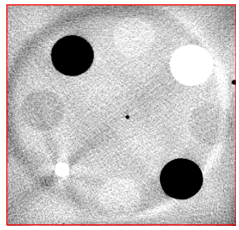

(g) 20ms

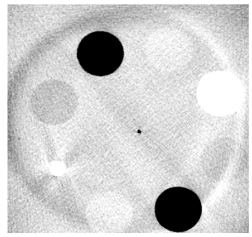

(h) 32ms

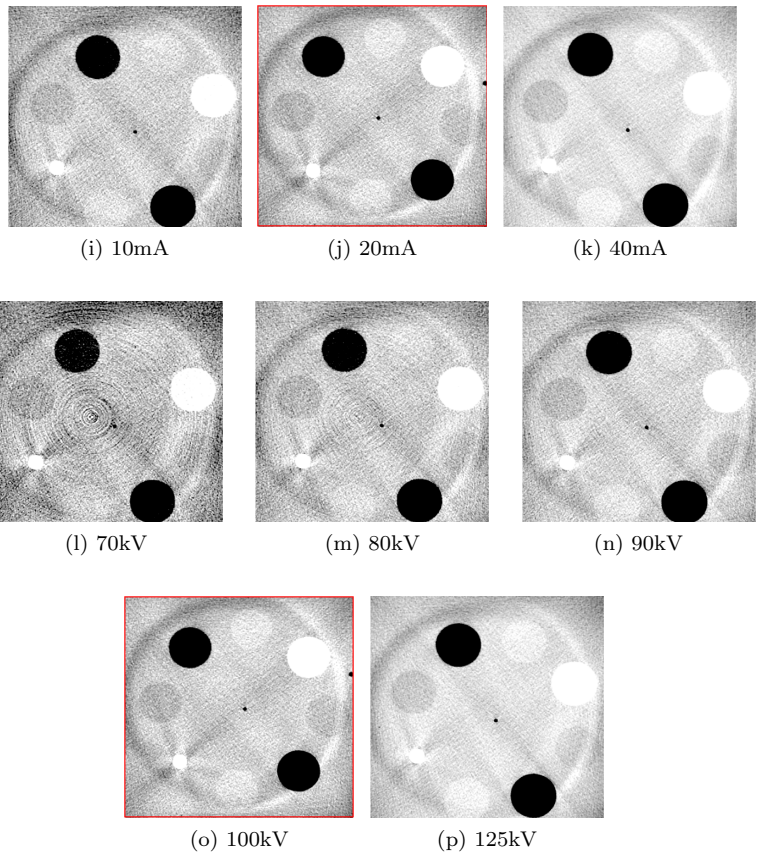

(i) 10mA (j) 20mA (k) 40mA

(l) 70kV (m) 80kV (n) 90kV

(o) 100kV (p) 125kV

Figure 9.2: CBCT scan of the HDP varying slice thickness (a-c), ms (e-h), mA (i-k) and kV (l-p).

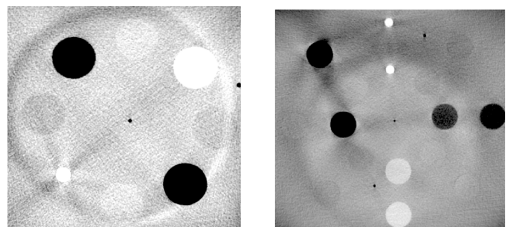

CBCT HDP S CBCT HDP S

Figure 9.3: CBCT scans obtained from HDP and PDP with standard scan protocols.

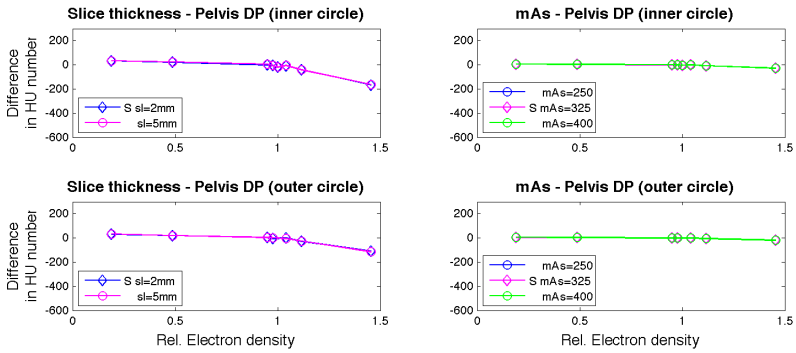

Figure 9.4: CT calibration curves obtained from the PDP, when varying slice thickness and mAs.

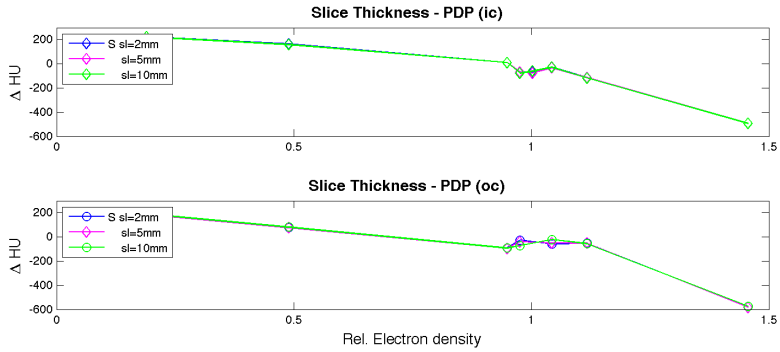

Figure 9.5: CBCT calibration curves obtained from PDP, when varying the slice thickness.

Chapter 10

Appendix B

10.1 Dose Calculations

10.1.1 ARP

Table 10.1: Statistical Results for ARP - PTV. (Abbreviations 6.1)

Procedure for Dose Calculation	PTV				Δ to CT %		
	$D_{2\%}$	$D_{98\%}$	Dmean	STD [Gy]	$D_{2\%}$	$D_{98\%}$	Dmean
CT							
CTS_CTS	104.2	96.2	68.9	1.3			
CTS_Def	104.1	95.7	68.7	1.4	0.3	0.6	0.3
CBCT							
CBS_ CTS	104.1	95.9	68.8	1.3	0.2	0.3	0.1
CBS_CBS	104.1	96.0	68.8	1.3	0.2	0.3	0.1
CBHq_CTS	104.4	95.8	68.7	1.4	-0.2	0.4	0.2
CBHq_CBHq	104.7	96.0	69.0	1.4	-0.4	0.2	-0.2
CBLd_CTS	103.8	92.9	68.3	1.8	0.4	0.3	0.8
CBLd_CBLd	103.6	92.8	68.2	1.7	0.6	0.4	1.0

Table 10.2: Statistical Results for ARP - OAR. (Abbreviations 6.1)

Procedure for Dose calculation	Medulla D_{max}	STD [Gy]	Δ to CT %	Medulla PRV D_{max}	STD [Gy]	Δ to CT %
CT						
CTS_CTS	43.9	4.4		49.2	6.7	
CTS_Def	43.8	4.4	0.3	50.0	6.7	-1.6
CBCT						
CBS_CTS	44.0	4.1	-0.2	50.4	6.3	-2.5
CBS_CBS	44.0	4.1	-0.2	50.4	6.2	-2.5
CBHq_CTS	44.7	3.5	-1.7	52.7	6.0	-7.1
CBHq_CBHq	44.8	3.5	-2.0	53.0	6.0	-7.7
CBLd_CTS	43.9	4.6	0.1	54.4	6.9	-10.5
CBLd_CBLd	43.8	4.6	0.3	54.2	6.8	-10.2

Table 10.3: Statistical Results for ARP - OAR. (Abbreviations 6.1)

Procedure for Dose calculation	Left Parotis D_{mean}	STD [Gy]	Δ to CT % D_{mean}
CT			
CTS_CTS	24.8	13.6	
CTS_Def	24.8	13.6	
CBCT			
CBS_CTS	25.7	13.1	-3.5
CBS_CBS	25.7	13.1	-3.5
CBHq_CTS	25.6	13.9	-3.4
CBHq_CBHq	25.7	13.9	-3.5
CBLd_CTS	19.5	10.2	21.6
CBLd_CBLd	19.4	10.2	21.7

10.1.2 H&N

Table 10.4: Statistical Results for H&N -PTV. (Abbreviations 6.1)

	PTV			Δ to CT %		
Procedure for	$D_{2\%}$	$D_{98\%}$	Dmean	D_2	$D_{98\%}$	Dmean
Dose calculation						
CT						
CTS_CTS	103.4	97.7	68.7			
CTS_Def	103.0	97.0	68.1	0.4	0.7	0.9
CBCT						
CBS_Def	103,1	96.0	67.6	0.3	1.7	1.6
CBS_CTS	103.6	97.8	68.5	-0.2	-0.1	0.2
CBS_CBS	103.1	98.0	68.8	0.2	-0.3	-0.2
CBp_CBpoc	102.0	94.3	65.8	-0.9	1.9	1.2

Table 10.5: Statistical Results for H&N - Medulla. (Abbreviations 6.1)

Procedure for Dose calculation	Medulla D_{max}	Δ to CT %	Medulla PRV D_{max}	Δ to CT %
CT				
CTS_CTS	42.3		50.0	
CTS_Def	42.2	0.2	49.8	0.4
CBCT				
CBS_CTS	42.5	-0.3	49.5	0.9
CBS_CBS	42.5	-0.5	50.0	-0.1
CBS_CBpic	44.3	1.6	48.7	0.1
CBS_CBpoc	44.2	1.8	48.7	1.1

Table 10.6: Statistical Results for H&N - Left Parotis. (Abbreviations 6.1)

Procedure for Dose calculation	Left Parotis D_{mean}	STD [Gy]	Δ to CT % D_{mean}
CT			
CTS_CTS	52.7	14.1	
CTS_Def	52.3	14.0	0.7
CBCT			
CBS_CTS	52.5	14.0	0.4
CBS_CBS	52.2	14.3	1.1
CBS_CBppic	51.7	13.9	2.0
CBS_CBpoc	54.4	14.2	-3.1

10.2 Cervix

Table 10.7: Statistical Results for Cervix - PTV. (Abbreviations 6.1)

Procedure for Dose Calculation	PTV $D_{2\%}$	$D_{98\%}$	D_{mean}	Δ to CT % D_2	$D_{98\%}$	D_{mean}
CT						
CTp_CTpoc	101.1	89.8	60.3			
CTp_Def	102.5	96.6	59.1	-1.4	-7.5	2.0
CBCT						
CBp_CTpoc	101.4	95.4	59.7	-0.3	-6.2	1.1
CBp_CBpoc	99.9	93.9	58.7	1.2	-4.5	2.6

Table 10.8: Statistical Results for Cervix - Caput Femoris. (Abbreviations 6.1)

Procedure for Dose calculation	Right Caput Fem D_{max}	Δ to CT %	Left Caput Fem D_{max}	Δ to CT %
CT				
CTp_CTpoc	49.6		46.5	
CTp_Def	49.0	1.2	51.1	-9.9
CBCT				
CBp_CTpoc	49.0	1.3	50.4	-8.4
CBp_CBpoc	48.0	3.0	49.5	-6.4

Table 10.9: Statistical Results for Cervix - Intestine. (Abbreviations 6.1)

Procedure for Dose calculation	Intestine V_{45Gy}	Δ to CT %
CT		
CTp_CTpo	148.5	
CTp_Def	155.6	-4.6
CBCT		
CBp_CTpoc	139.6	6.0
CBp_CBpoc	128.9	13.2

Bibliography

[1] http://www.toboc.com/Thermoplastic-Mask-S-Shaped-Head-Neck-Shoulder-Mask/703044-242335-Exporter-TradeLead.aspx.

[2] http://www.smithersmedicalproducts.com/alphacradle/patientscatalog/products.htm.

[3] http://www.cirsinc.com/.

[4] http://www.rsdphantoms.com/rt_art.htm.

[5] http://www.dahanca.dk/get_media_file.php?mediaid=57.

[6] http://www.varian.com/dyna/onco-summit2011/Presentations/Session8/8_1_Elstroem_Adaptive_Treatment_Strategies_in_HN_and_Pelvic_Regions.pdf.

[7] Mary ES Beaver, Keith E. Matheny, Dianna B. Roberts, and Jeffrey N. Myers. Predictors of weight loss during radiation therapy. *Otolaryngology - Head and Neck Surgery*, 125(6):645 – 648, 2001.

[8] J.T. Bushberg. *The essential physics of medical imaging.* Williams & Wilkins, 2002.

[9] P. Castadot, J.A. Lee, X. Geets, and V. Grégoire. Adaptive radiotherapy of head and neck cancer. In *Seminars in radiation oncology*, volume 20, pages 84–93. Elsevier, 2010.

[10] G.T.Y. Chen, G.C. Sharp, and S. Mori. A review of image-guided radiotherapy. *Radiological Physics and Technology*, 2(1):1–12, 2009.

[11] KY Cheung. Intensity modulated radiotherapy: advantages, limitations and future developments. *Biomed. Imag. Intervent. J*, 2:1–19, 2006.

[12] Z.H. Cho, J.P. Jones, and M. Singh. Foundations of medical imaging. *Recherche*, 67, 1993.

[13] RE Drzymala, R. Mohan, L. Brewster, J. Chu, M. Goitein, W. Harms, and M. Urie. Dose-volume histograms. *International Journal of Radiation Oncology* Biology* Physics*, 21(1):71–78, 1991.

[14] U.V. Elstroem, L.P. Muren, J.B.B. Petersen, and C. Grau. Evaluation of image quality for different kv cone-beam CT acquisition and reconstruction methods in the head and neck region. *Acta Oncologica*, 50(6):908–917, 2011.

[15] M. Goitein. The comparison of treatment plans. In *Seminars in Radiation Oncology*, volume 2, pages 246–256. Elsevier, 1992.

[16] J.W. Goldwein. Radiation myelopathy: a review. *Medical and pediatric oncology*, 15(2):89–95, 1987.

[17] C. Grau. Damage to the spinal medulla caused by radiation]. *Ugeskrift for laeger*, 155(4):208, 1993.

[18] V. Gregoire and TR Mackie. State of the art on dose prescription, reporting and recording in intensity-modulated radiation therapy (ICRU report no. 83). *Cancer/Radiotherapy*, 2011.

[19] E.K. Hansen, M.K. Bucci, J.M. Quivey, V. Weinberg, and P. Xia. Repeat ct imaging and replanning during the course of IMRT for head-and-neck cancer. *International Journal of Radiation Oncology* Biology* Physics*, 64(2):355–362, 2006.

[20] L.B. Harrison, R.B. Sessions, and W.K. Hong. *Head and neck cancer: a multidisciplinary approach*. Lippincott Williams & Wilkins, 2008.

[21] J. Hatton, B. McCurdy, and P.B. Greer. Cone beam computerized tomography: the effect of calibration of the hounsfield unit number to electron density on dose calculation accuracy for adaptive radiation therapy. *Physics in medicine and biology*, 54:N329, 2009.

[22] Onkologisk afdeling R Herlev hospital. *Strålebehandling i hoved-og hals området*, 2010.

[23] C.C. Hu, W.T. Huang, C.L. Tsai, J.K. Wu, H.L. Chao, G.M. Huang, C.W. Wang, C.J. Wu, and J.C.H. Cheng. Practically acquired and modified cone-beam computed tomography images for accurate dose calculation in head and neck cancer. *Strahlentherapie und Onkologie*, pages 1–12, 2011.

[24] D. Jaffray, P. Kupelian, T. Djemil, and R.M. Macklis. Review of image-guided radiation therapy. *Expert review of anticancer therapy*, 7(1):89–103, 2007.

[25] W.A. Kalender. *Computed tomography: fundamentals, system technology, image quality, applications*. Wiley-VCH, 2011.

[26] C.H. Kau, K. Abramovitch, S.G. Kamel, and M. Bozic. *Cone beam CT of the head and neck: an anatomical atlas*. Springer, 2011.

[27] R. Larsen. 02505 course note, medical image analysis. 2008.

[28] AC Miracle and SK Mukherji. Conebeam CT of the head and neck, part 1: physical principles. *American Journal of Neuroradiology*, 30(6):1088–1095, 2009.

[29] J.C. O'Daniel, A.S. Garden, D.L. Schwartz, H. Wang, K.K. Ang, A. Ahamad, D.I. Rosenthal, W.H. Morrison, J.A. Asper, L. Zhang, et al. Parotid gland dose in intensity-modulated radiotherapy for head and neck cancer: is what you plan what you get? *International Journal of Radiation Oncology* Biology* Physics*, 69(4):1290–1296, 2007.

[30] E.B. Podgorsak. Review of radiation oncology physics: a handbook for teachers and students. *Review of radiation oncology physics: a handbook for teachers and students*, 2003.

[31] Moeslund B.T. Poulsen, R. R. *Introduction to Medical Image Analysis*. DTU informatics, 2011.

[32] J.A. Purdy, J.M. Michalski, J. Bradley, S. Vijayakumar, C.A. Perez, and S.H. Levitt. Three-dimensional treatment planning and conformal therapy. *Technical Basis of Radiation Therapy*, pages 179–202, 2006.

[33] A. Richter, Q. Hu, D. Steglich, K. Baier, J. Wilbert, M. Guckenberger, and M. Flentje. Investigation of the usability of conebeam CT data sets for dose calculation. *Radiat Oncol*, 3(1):42, 2008.

[34] Y. Rong, J. Smilowitz, D. Tewatia, W.A. Tomé, and B. Paliwal. Dose calculation on kv cone beam CT images: an investigation of the HU-density conversion stability and dose accuracy using the site-specific calibration. *Medical Dosimetry*, 35(3):195–207, 2010.

[35] W.C. Scarfe and A.G. Farman. What is cone-beam CT and how does it work? *Dental Clinics of North America*, 52(4):707–730, 2008.

[36] R. Schulze and U. Heil. Artefacts in CBCT: a review. *Dentomaxillofacial Radiology*, 40(5):265–273, 2011.

[37] D.L. Schwartz and L. Dong. Adaptive radiation therapy for head and neck cancer—can an old goal evolve into a new standard? *Journal of oncology*, 2011, 2011.

[38] J. Seco and PM Evans. Assessing the effect of electron density in photon dose calculations. *Medical physics*, 33:540, 2006.

[39] Varian Medical systems. On-board imager (OBI) reference guide,. 2008.

[40] Varian Medical systems. Eclipse algorithms reference guide. 2009.

[41] S. Webb and D. McQuaid. Some considerations concerning volume-modulated arc therapy: a stepping stone towards a general theory. *Physics in medicine and biology*, 54:4345, 2009.

[42] N. Wen, H. Guan, R. Hammoud, D. Pradhan, T. Nurushev, S. Li, and B. Movsas. Dose delivered from varian's cbct to patients receiving imrt for prostate cancer. *Physics in medicine and biology*, 52:2267, 2007.

[43] I.M.R.T.C. Working et al. Intensity-modulated radiotherapy: current status and issues of interest. *International Journal of Radiation Oncology* Biology* Physics*, 51(4):880–914, 2001.

[44] I.M.R.T.C. Working et al. Prescribing, recording, and reporting photon-beam intensity- modulated radiation therapy (IMRT). *Journal of the ICRU report 83*, 10(1), 2010.

[45] Y. Yang, E. Schreibmann, T. Li, C. Wang, and L. Xing. Evaluation of on-board kv cone beam CT (CBCT)-based dose calculation. *Physics in medicine and biology*, 52:685, 2007.

[46] B. Zitova and J. Flusser. Image registration methods: a survey. *Image and vision computing*, 21(11):977–1000, 2003.